Materials Science and Engineering, R21 (1997) 47–100

Reports: A Review Journal

Review of advances in cubic boron nitride film synthesis

P.B. Mirkarimi *, K.F. McCarty, D.L. Medlin
Sandia National Laboratories, Livermore, CA 94550, USA

Abstract

Cubic boron nitride (cBN) has a number of highly desirable mechanical, thermal, electrical, and optical properties. Because of this, there has been an extensive worldwide effort to synthesize thin films of cBN. Film synthesis is difficult in that without significant levels of ion bombardment during growth, only sp2-bonded BN forms, not sp3-bonded cBN. Recently there has been considerable progress in improving the deposition techniques and cBN film quality. In addition, progress has been made in understanding how energetic deposition conditions can lead to cBN formation. However, unanswered questions remain and process improvements are still needed. In this paper we critically and comprehensively review recent developments in cBN film synthesis and characterization. First, the structures and stability of the BN phases and characterization techniques are described. Next, the key experimental parameters controlling cBN film formation and synthesis techniques are discussed. Following a review of microstructure, the proposed mechanisms of cBN formation and the observed mechanical and electrical properties of cBN films are analyzed. We conclude by highlighting the current impediments to the practical realization of cBN-film technology. © 1997 Published by Elsevier Science S.A.

Keywords: Cubic boron nitride; c-BN; Films; Deposition; Characterization; Mechanisms

1. Introduction

The cubic phase of boron nitride (cubic BN or cBN) has significant technological potential for thin-film applications. Having a Vickers hardness of about 5000 kg mm^{-2}, cBN is second in hardness only to diamond [1–3] and hence is a natural candidate for hard, protective coatings. The fact that cBN (i) does not react readily with ferrous metals [1] (as does diamond [4]), (ii) can be deposited in thin-film form at low temperatures (unlike diamond [4]), and (iii) has a high resistance to oxidation [1,5] (at temperatures as high as 1300 °C) makes it even more attractive for tooling applications. Cubic BN is transparent in the infrared [6] and visible [1] parts of the spectrum, and thus is sought after as a protective coating for optical elements.

Because of its wide bandgap [1] ($E_g \approx 6$ eV) and good thermal conductivity [1], cubic BN also has the potential for the same high-temperature and high-power electronic applications envisioned for diamond films. Furthermore, unlike diamond films, cBN has been doped *both* p- and n-type [7,8], and can be passivated with an oxide layer [9]. In fact, a photodiode emitting in the UV has been made from a p–n junction formed in bulk cubic BN [8,10].

BN films with a high ($>85\%$) percentage of the cubic phase can now be routinely deposited by a variety of techniques. In addition, our understanding of the experimental parameters that control phase selection in the BN system has advanced considerably over the last several years. However, barriers to technological implementation of cBN films remain. For example, the difficulty in depositing thick, adherent films under practical deposition conditions limits use of cBN as a hard, protective coating. Also, non-cubic BN phases tend to form before cBN is nucleated [11,12]. Because the

* Corresponding author. Present address: Lawerence-Livermore National Laboratory, Livermore, CA 94550.

0927-796X/97/$32.00 © 1997 Published by Elsevier Science S.A. All rights reserved
PII S0927-796X(97)00009-0

crystallinity is poor and epitaxial growth has not been achieved, electronic applications are not yet practical.

In this paper we critically and comprehensively review developments in cBN film synthesis and characterization, emphasizing work since the review paper written by Arya and D'Amico [13] in 1988. Reviews of different topics relating to cBN film synthesis have been subsequently published by Hackenberger et al., [14] Kulisch and Reinke [15], Richter [16], and Yoshida [17]. The reader is referred to these papers for additional information.

We first describe the structures and stability of the BN phases and review characterization techniques. Next, we highlight the most important experimental parameters controlling cBN film formation and survey synthesis techniques. Following a review of film microstructure, we discuss the proposed mechanisms of cBN formation and the observed mechanical and electronic properties of cBN films. We conclude by highlighting the current impediments to the practical realization of cBN-film technology. We summarize, in list form, a few key points at the end of each section.

- cBN films have many technologically desirable properties for hard-coating and electronic/photonic applications.
- cBN films have several advantages over diamond films.
- Despite recent progress, significant barriers still exist to commercializing cBN films.

2. Phases in the BN system

2.1. Structure

In many ways analogous to carbon, boron nitride forms both hard, diamond-like sp^3-bonded phases and softer, graphite-like sp^2-bonded phases. Crystal structure information and schematics for the four primary crystalline boron nitride phases are given in Table 1 and Fig. 1. A recent review of structural aspects of these phases has been given by Kurdyumov et al. [18]. The two equilibrium phases are the cubic, sp^3-bonded structure (cBN) [23] and the hexagonal, sp^2-bonded structure (hBN) [19]. cBN, which possesses the zinc-blende structure, consists of tetrahedrally coordinated boron and nitrogen atoms with {111} planes arranged in a three-layer (A B C ...) stacking sequence. hBN is a

Table 1
Structural data for the boron nitride phases

Phase	a (Å) [18]	c (Å) [18]	Space group	Atom positions
hBN [19]	2.5043	6.6562	$P6_3/mmc$ (194)	B: (0,0,0), (2/3,1/3,1/2) N: (2/3,1/3,0),(0,0,1/2)
rBN [20]	2.5042	9.99	R3m (160)	B: (0,0,0),(2/3,1/3,1/3), (1/2,2/3,2/3) N: (2/3,1/3,0),(1/3,2/3,1/3), (0,0,2/3)
cBN [1,21]	3.6153		$F\bar{4}3m$ (216)	B: (0,0,0), (1/2,1/2,0), (0,1/2,1/2), (1/2,0,1/2) N: (1/4,1/4,1/4), (3/4,3/4,1/4),(1/4,3/4,3/4), (3/4,1/4,3/4)
wBN [21,22]	2.5505	4.210	$P6_3mc$ (186)	B: (0,0,0), (1/3,2/3,1/2) N: (0,0,3/8), (1/3,2/3,7/8)

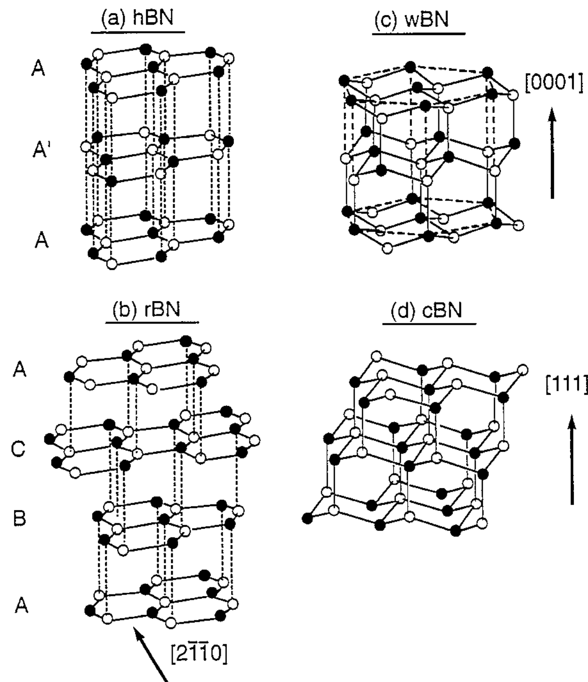

Fig. 1. Structures of the sp^3-bonded phases cBN and wBN and the sp^2-bonded phases hBN and rBN.

layered structure that is similar to graphite with the exception that hexagonal rings of the basal planes in hBN are positioned directly above each other and rotated by 180° between alternate layers. The two-layer (0002) stacking sequence for hBN can thus be described as A A ′ A... [19].

These stacking sequences can vary for both the sp^2- and sp^3-bonded phases producing additional sp^3- and sp^2-bonded polytypes that are metastable. For instance, the stacking relationship between the sp^3-bonded cubic and wurtzitic (wBN) [24] phases of boron nitride is analogous to that between cubic and hexagonal diamond (Lonsdaleite). Specifically, wBN consists of a two-layer (A A ′ A...) stacking of (0002) planes (which are structurally identical to the cBN {111} planes). Similarly, with all the planes oriented in the same rotational sense, rearrangement of the basal planes of sp^2-bonded BN in a staggered A B C... stacking arrangement yields an additional phase, rhombohedral boron nitride (rBN) [25,20], which is structurally analogous to rhombohedral graphite [26]. As is discussed below, the similar stacking between cBN and rBN and between wBN and hBN plays an important role in bulk-phase transformations.

As with graphitic carbon, sp^2-bonded boron nitride often is found in a disordered, turbostratic form (tBN). This is the form of sp^2-bonded material most commonly observed in boron nitride thin films. For a turbostratic structure, the two-dimensional in-plane order of the hexagonal basal planes is largely retained, but these planes are stacked in a random sequence and with random rotation about the *c* axis. Turbostratic BN was studied extensively by Thomas et al. [27] and, as is discussed in Section 3.2, produces a broad and diffuse diffraction pattern that is distinct from that for hexagonal and rhombohedral boron nitride. Accompanying this decrease in stacking order is a general increase in the (0002) interplanar spacing (i.e. the basal-plane separation) [18,27] as well as a decrease in the in-plane coherence length. In fact, it is difficult to identify well defined crystallites of tBN. Instead, the basal planes remain continuous as they bend through a wide range of orientations. Fig. 2 shows a high resolution transmission electron microscopy image (see Section 3.3) of a tBN film.

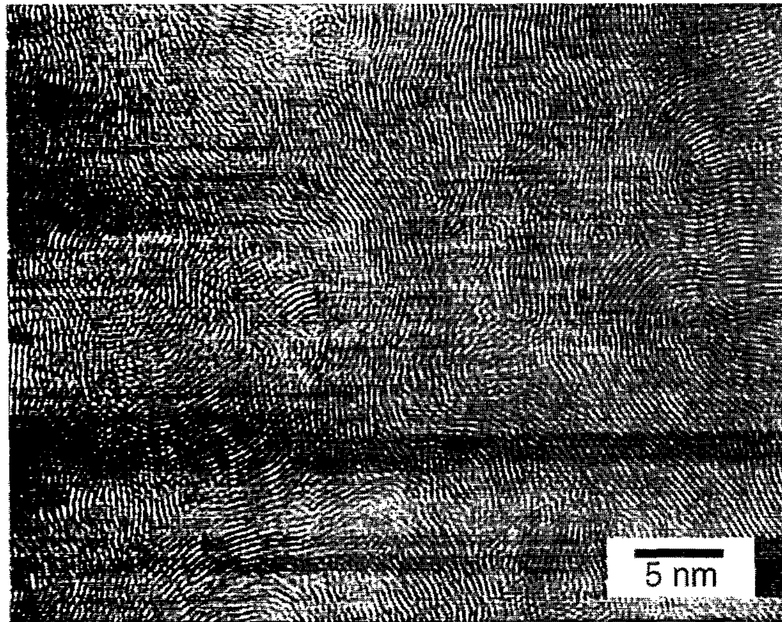

Fig. 2. High resolution transmission electron microscopy (HRTEM) image of a tBN film in plan view. The majority of contrast is lattice fringes from the basal planes of the poorly crystalline, graphitic material. The basal planes are highly distorted and extend only over a short distance. From McCarty et al. [28]

2.2. Phase stability

Cubic boron nitride is commercially synthesized in bulk form by the application of high pressures and temperatures. Recent articles have reviewed the status of high-temperature/high-pressure synthesis [29]. The original development of the pressure–temperature (P–T) phase diagram [24,30] indicated, in analogy with the diamond-graphite system, that graphitic BN (hBN) is thermodynamically stable at ambient temperatures and pressures, whereas the cubic phase is only stable at high pressures. However, recent experiments and calculations [31–33] suggest that the P–T phase boundary line should be shifted to lower pressure, which would make cBN the thermodynamically stable phase under ambient conditions. Regardless of the exact position of the thermodynamic equilibrium line, a significant kinetic barrier hinders the direct transition from sp^2 to sp^3 bonding under ambient conditions. Furthermore, upon application of pressure at low temperatures the phase that is formed depends sensitively on the precursor material. For instance, because of the similarities in stacking sequence, under pressure well-ordered hBN transforms to wBN, whereas rBN transforms to cBN [34]. For both cases, these transitions occur at room temperature only after application of pressures well above even the Bundy–Wentorf line (hBN $\rightarrow$ wBN, $P > 11$ GPa [24,32]; rBN $\rightarrow$ cBN, $P > 8$ GPa [35]). Thus, as will be discussed in the following sections, synthesis of cBN films requires significant processing measures to overcome these kinetic or thermodynamic barriers.

- The primary BN phases are sp^3-bonded cBN and wBN, and sp^2-bonded hBN, rBN, and tBN, a disordered form of hBN.
- cBN is a diamond-like material with a zinc-blende crystal structure.
- There is a kinetic barrier to cBN formation under ambient conditions regardless of whether cBN is thermodynamically metastable or stable under ambient conditions.

3. Characterization techniques

As described by McKenzie et al. [36], characterization of BN films is non-trivial, and conclusive phase identification requires application of several complementary techniques. In part this is because thin-film cBN is typically very small grained and highly defective. In this section, we describe the attributes, including the limitations, of the common characterization techniques.

3.1. Fourier transform infrared spectroscopy

Because it gives ready estimates of cBN content, the most important and widely used tool for characterizing BN films is Fourier transform infrared (FTIR) spectroscopy. FTIR analysis is a straightforward, non-destructive, and rapid technique that can be done in either reflection or transmission.

3.1.1. Phase identification with FTIR spectroscopy

Being vibrational spectroscopies, infrared and Raman spectroscopies are sensitive to the bonding of BN films. For crystalline materials, the techniques only sample the vibrational modes (i.e. the phonons) near the center of the Brillouin zone (i.e. phonon wavevector ≈ 0) [37]. For near-normal incidence of thin films, IR reflection and transmission gives peaks near the frequency of the vibration modes in their transverse optical (TO) polarization. As the film becomes thick, light between the longitudinal optical (LO) and TO frequencies cannot be transmitted through the lattice. This produces a *reststrahlen* band of high reflectivity (or low transmission) between the LO and TO frequencies [37]. This thick-film peak is broadened and upshifted in frequency from the peak of a thin film. Defects can also change the IR absorbances. For both Raman and infrared spectroscopy, as the crystallinity is reduced, the selection rules that allow only the near-zone-center phonons to be observed break down, leading to broadening and shifting of the peaks. The broadening can be quite pronounced for amorphous materials, where the entire density of vibrational states can contribute to the IR and Raman spectra [38].

The vibrational properties of single-crystal cBN and highly crystalline hBN are well known (see Table 2) while those of rBN and wBN are not well investigated. Unfortunately, only micron-scale, highly defective powders of wBN are available for bulk studies. Since the vibrational frequencies are sensitive to the bonding type, similarities in the IR peaks of rBN and hBN, and wBN and cBN are expected. Therefore, while it is straightforward to distinguish sp^2-bonded from sp^3-bonded BN, it is more difficult to distinguish *between* sp^2 phases (say hBN vs. rBN) or sp^3 phases (cBN vs. wBN). For cBN, the single, triply degenerate phonon is both IR (see Fig. 3(a)) and Raman active (see Fig. 3(b)) and is split into a TO component at ~ 1060 cm^{-1} and an LO component at ~ 1310 cm^{-1} by the ionicity of the crystal. For hBN, the two IR-active phonons have TO frequencies at about ~ 780 and ~ 1370 cm^{-1}, respectively (see Fig. 3(c)) [42]. The 1370 cm^{-1} mode is a stretching of the B–N bond *within* the basal plane, and the 780 cm^{-1} mode is a bending of the B–N–B bond *between* the basal planes. rBN has two vibration modes, both of which are Raman and infrared active. These modes are closely related to the IR-active modes of hBN[1] and have been found by Raman analysis at essentially the same frequencies as the IR-active modes of hBN [44,45]. Therefore, the IR spectra of hBN and

[1] The A_1 and E modes of rBN involves vibration of the B and N atoms between and within, respectively, the basal planes. These modes are similar to the A_{2u} and E_{1u} modes, respectively, of hBN and graphite. More exactly, the rBN A_1 mode has the same atomic displacements as one of the 'silent' B_{1g} modes of hBN and graphite. The rBN E mode has the same atomic displacements as the one of the E_{2g} modes of hBN and graphite. The atomic displacements are given pictorially as the modes labeled 'B_{1g2}' and 'E_{2g2}' in Ref. [47]. In graphite [47], and presumably in hBN, the out-of-plane B_{1g} and A_{2u} modes have essentially the same frequency as the in-plane E_{2g} and E_{1u} modes. Because of this, the A_1 and E modes of rBN occur, respectively, at essentially the frequency as the A_{2u} and E_{1u} modes of hBN.

Table 2
Optical vibrational modes of cBN, wBN, hBN, and rBN

Crystal structure	Activity [b]	Mode symmetry	Measured frequencies [a]	
			Infrared	Raman
cBN	R, IR	F_2 TO	1065 [6], ~1050 [39]	1056 [40]
		F_2 LO	1340 [6], ~1310 [39]	1304 [40]
wBN	R, IR	A_1 TO		950 [41] [d]
		A_1 LO	1090 [41] [c]	1015 [41] [d]
	R, IR	E_1 TO	1120 [41] [c]	1050 [41] [d]
		E_1 LO	1230 [41] [c]	1295 [41] [d]
	R	E_2		
	R	E_2		
	silent	B_1		
	silent	B_1		
hBN	IR	A_{2u} TO	783 [42]	
		A_{2u} LO	828 [42]	
	silent	B_{1g}		
	silent	B_{1g}		
	IR	E_{1u} TO	1367 [42]	
		E_{1u} LO	1610 [42]	
	R	E_{2g}		52 [43]
	R	E_{2g}		1366–1370 [42,43]
rBN	R, IR [290]	A_1 TO		790 [44,45] [e]
		A_1 LO		
	R, IR [290]	E TO		1367 [44,45] [e]
		E LO		

[a] All frequencies in cm^{-1}.
[b] R, Raman active; IR, infrared active; silent, not infrared or Raman active.
[c] Frequencies are tentative and no assignments to modes are possible. wBN should have only two TO IR-active modes, yet both Doll [41] and Kessler et al. [46] observed three transmission peaks from wBN powders.
[d] Frequencies are tentative and no assignments to modes are possible.
[e] Assignment to TO polarization is tentative.

rBN will be quite similar (subtle differences between rBN and hBN have been presented by Doll [48]). Poorly crystalline sp^2-bonded BN (i.e. tBN) has the same two IR peaks as hBN and rBN, except broadened.

wBN has two IR-active modes. Both Kessler et al. [46] and Doll [41] found peaks in IR transmission at about 1085, 1125, and 1250 cm^{-1}, with the first peak being the most intense. Until the vibrational properties of wBN are better known, the secondary peaks around 1125 and 1250 cm^{-1} can be used to distinguish cBN from wBN. In summary, a reasonably symmetric IR peak near 1060 cm^{-1}

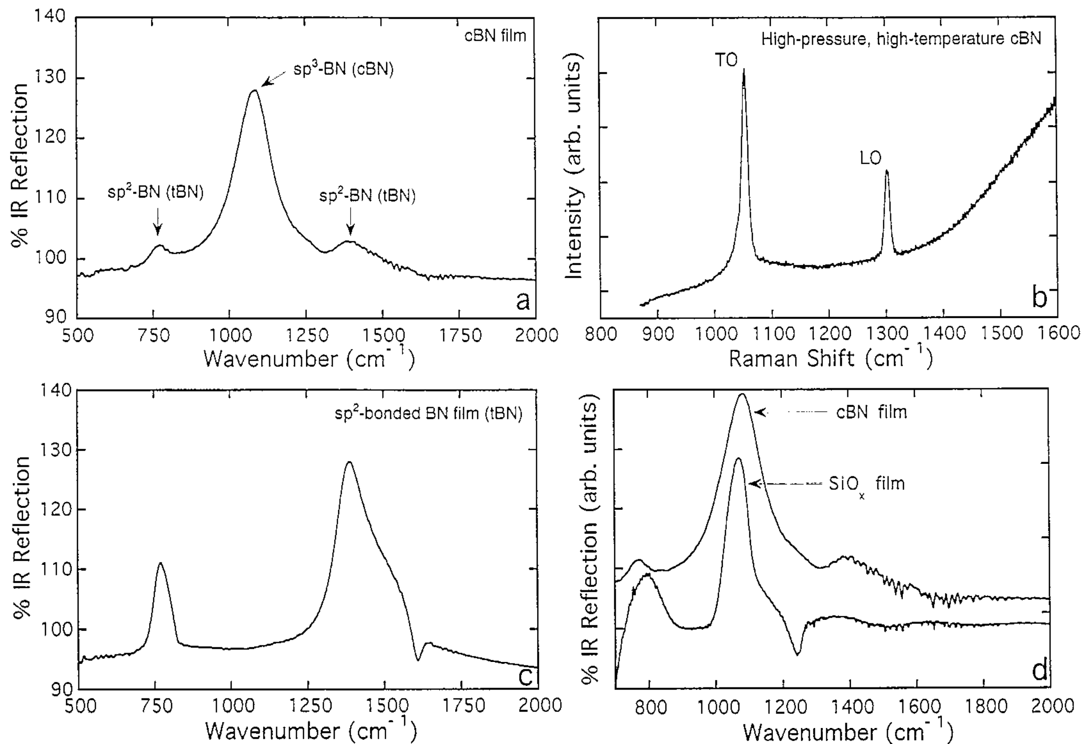

Fig. 3. Vibrational spectroscopy of BN phases. (a) FTIR spectrum for an ~1000 Å thick film with a high cBN fraction taken in reflection and ratioed to the spectrum of an uncoated silicon substrate. (b) Raman spectrum of a commercial, sintered compact of cBN grains synthesized at high temperature and pressure. Obtained using a 514.5 nm laser. (c) FTIR spectrum for an sp^2-bonded BN film (tBN) taken in reflection and ratioed to the spectrum of an uncoated silicon substrate. (d) Comparison of FTIR spectra from a mainly cBN film and a SiO_x film, the latter being the oxide 'seal' coat on the back side of a commercial Si(100) wafer. Both spectra taken in reflection and are ratioed to the spectrum of a clean silicon substrate.

is the vibrational fingerprint of thin-film cBN, while peaks near 780 and 1370 cm^{-1} are the fingerprints of sp^2-bonded BN.

Information on the orientation of the basal planes in hBN/tBN relative to the substrate can be inferred [49–51] from the ratio of the IR peak intensity at ~780 cm^{-1} (I_{780}) to the peak intensity at ~1370 cm^{-1} (I_{1370}). For near-normal incidence of IR light, the out-of-plane mode (780 cm^{-1}) is enhanced relative to the in-plane mode (1370 cm^{-1}) as the basal planes orient themselves perpendicular to the substrate (c axis parallel to substrate). Likewise, as the basal planes become oriented parallel to the substrate, the ratio of I_{780}/I_{1370} will decrease.

3.1.2. Pitfalls in phase identification by IR spectroscopy

Although IR analysis is a powerful technique for phase identification, it must be done carefully. There are many examples in the literature where the existence of cBN has been wrongly concluded because the IR spectroscopy was misinterpreted. Extreme examples include confusing the well-known IR absorbances of hBN/tBN with those of cBN [52]. Most misidentification occurs, however, when non-BN features near 1060 cm^{-1} are assigned to cBN. For silicon substrates, in particular, there is an intense IR absorption associated with SiO_x between about 1100 and 1050 cm^{-1}, depending on the oxygen content [53]. This feature has a shoulder at about 1150 cm^{-1} that is also dependent on oxygen content. These features can be misinterpreted as the signature of cBN (see Fig. 3(d)). Under typical deposition conditions (i.e. some substrate cleaning and deposition in a low oxygen environment), any SiO_x layer will be reasonably thin (less than tens of angströms) and its presence will not be a significant

issue unless the BN film is also very thin. Furthermore, if truly from cBN, a peak near 1060 cm^{-1} will exhibit systematic behavior such as increasing in intensity with increasing film thickness.

3.1.3. Quantitative estimates of cBN content

Infrared spectroscopy is widely used for determining relative amounts of cBN in BN films. Precise quantification is non-trivial mainly because the complex microstructure makes determination of the optical 'constants' of cBN and particularly tBN problematic. In general, the reflection or transmission of IR light through a thin film on a substrate is a complicated process that is sensitive to the film thickness (interference effects), angle of incidence, and the optical constants of the film and the substrate. Even for fixed optical properties, changing film thickness and incidence angle can lead to frequency shifts, intensity variations, and line-shape distortions, particularly for reflectance spectra [54].

Several approaches for phase quantification have been presented in the literature. For both reflection or transmission analysis, it is common to assume that:

$$\text{volume fraction cBN} \approx \frac{I_{1060}}{I_{1060} + I_{1370}} \tag{1}$$

where I_{1060} and I_{1370} are the normalized reflected or transmitted intensities (i.e. the ratio of the reflected or transmitted intensity to the incident intensity) of the IR absorbances at approximately 1060 and 1370 cm^{-1}, respectively. For *reflectance* spectra of films on *silicon* substrates, this relationship has some theoretical justification. Friedmann et al. [55] modeled the infrared response of thin cBN, hBN, and intimately mixed hBN/cBN films on silicon substrates using the optical constants for highly crystalline cBN and hBN. The hBN was assumed to be randomly oriented, and therefore, the estimates of cBN content may be high if the tBN is aligned with its basal planes perpendicular to the substrate. If the interfaces are smooth and sharp, the simulations include the effect of the substrate on the complex refractive index of the film near resonance frequencies and multiple reflection effects. For mixed-phase films between about 500 and 2000 Å thick, they found that the volume fraction of cBN was approximately within (order 5% accuracy) that given by Eq. (1). Simulations of layered structures (e.g. Si/hBN/cBN) and/or oriented hBN is straightforward in this approach. BN films on metallic substrates [56] have also been simulated. The importance of the substrate is illustrated in that the intensity ratio of Eq. (1) needed to be multiplied by about 1.4 to estimate cBN content on metallic substrates. The principal deficiency of such analyses is the use of the optical constants of *highly crystalline* cBN and hBN. Because the cBN grains are nanocrystalline and highly defected, and the tBN is very poorly crystalline and can be highly oriented, BN films can have optical properties that are significantly different from single-crystal cBN and pyrolytic hBN. For example, the absorption coefficients of cBN and tBN in films are much less than those predicted from the nearly single-crystal properties [57,58].

For transmission analysis, approaches for quantification based upon the film absorbance have been proposed.[2] Absorbance is the logarithm of the ratio of the incident intensity to the transmitted intensity. The absorption coefficient $\alpha(\omega)$ is the frequency-dependent absorbance divided by the film thickness. These approaches correctly account for the exponential loss of intensity with pathlength (i.e. the Lambert–Beer law) but typically neglect the substrate. [3] The work of Jäger et al. [57] shows that the first assumption is crude at best, most likely leading to overestimating the cBN content.

[2] In spectral regions of strong phonon absorbances, in general, there is no simple relationship between the reflected and transmitted intensity of a film on a substrate.

[3] For transmission analysis, Eq. (1) is valid only for two conditions: (1) the absorption coefficient of cBN at ~1060 cm^{-1} is equal to the absorption coefficient of hBN/tBN at ~1370 cm^{-1}, and (2) the film is thin enough that the linear approximation of the Lambert–Beer law is valid.

Yokoyama et al. [59] proposed a relationship between the volume ratio of cBN and tBN/hBN based on the absorption coefficients calculated from the optical properties of highly crystalline cBN and hBN. Jäger et al. [57] improved this relationship by correctly accounting for the densities of hBN and cBN and by measuring the absorption coefficients of the tBN and cBN. tBN films of known thickness were analyzed using an approach that has been applied to quantify the hydrogen content in amorphous, tetrahedrally bonded semiconductors. The procedure gave a 'calibration' constant that related the measured *integrated* absorption to the number density of hBN/tBN oscillators. Not having pure cBN films, both the calibration constant of cBN and the cBN content were inferred by analysing mixed-phase tBN/cBN films of known thickness. A simple linear relationship was found between the absorption coefficient ratios and the inferred volume fractions of cBN and tBN. Specifically, if f_{cBN} and f_{tBN} are the volume fractions of cBN and tBN, respectively, then $f_{cBN}/f_{tBN} = 0.6 \times \alpha(1060\ \mathrm{cm}^{-1})/\alpha(1370\ \mathrm{cm}^{-1})$ [4] and $f_{cBN}/f_{tBN} = 0.19 \times \alpha(1060\ \mathrm{cm}^{-1})/\alpha(780\ \mathrm{cm}^{-1})$. Even though Jäger et al. measured an absorption constant, determining the 'best' absorption coefficient (and thus the multiplicative constant) for the sp^2-bonded BN is still problematic. The microstructure, specifically the extent of preferred orientation, in an sp^2-bonded reference film grown with insufficient ion flux to make cBN may be quite different from the highly oriented tBN found in the interfacial layer of cBN-containing films (see Section 6). For example, Tsuda et al. [58] found that α_{1370} changed by nearly a factor of three for a modest change in substrate bias.

Improved quantitative analysis using IR spectroscopy requires that the substrate be accounted for and that the optical constants for cBN and tBN be determined by analysis. Friedrich et al. [60] have begun such work. This approach will also contribute to better characterizing the nature (e.g. extent of order and texture) of the tBN. For now, Eq. (1) can be applied to reflection analysis of thin films with the understanding that cBN content may be overestimated. For transmission analysis, the approach of Jäger et al. [57] can be applied with the proviso that the multiplicative constants are subject to refinement.

3.1.4. IR peak shifts

The FTIR peaks from cBN films are generally shifted to wavenumbers above the single crystal value of $\sim 1060\ \mathrm{cm}^{-1}$; this is commonly attributed to compressive stress. In fact, McKenzie et al. [61] observed that the IR peak of a cBN-containing film shifted from $1081\ \mathrm{cm}^{-1}$ to $1056\ \mathrm{cm}^{-1}$ after stress was relieved when the film delaminated from the substrate. Fahy [62,63] and Cardona and Anastassakis [64] have commented upon the shifts in frequency for the TO phonon of cBN for both isotropic and uniaxial strain. For uniaxial strain, the sign of the line shifts depended upon the direction of the strain axis relative to the phonon polarization. We caution that several other processes can shift the IR peaks, including film thickness [55], the degree of crystallinity, the optical properties of the substrate [56], and deviations in film stoichiometry [65]. In addition, Fahy et al. [66] have recently suggested that the shift in the cBN TO phonon observed during the initial nucleation [55,66] of cBN is largely not because of stress. Instead, they propose that geometrical factors (i.e. small discrete particles and their associated polarization field) resulting from island nucleation dominate the frequency shift. However, for stoichiometric films analyzed after the initial nucleation phase, the literature supports the notion that the IR peak of cBN in films occurs at wavenumbers higher than the bulk value because of compressive stress.

[4] The multiplicative constant 0.6 is nearly the density ratio of hBN to cBN. That is, the ratio of the absorption coefficients normalized by the appropriate densities approximately gives the volume ratio. Equivalently, the absorption coefficients measured by Jäger et al. [57] approximately scale with mass density.

3.2. Electron and X-ray diffraction methods

Because of the number of similarities in the interpretation of electron and X-ray diffraction (XRD) of boron nitride films, these two classes of techniques are discussed together. Several factors complicate the characterization of BN films by diffraction methods including small grain sizes and crystallographic disorder, overlap of reflections from multiple phases, and low scattering intensities.

Standard X-ray diffraction using conventional θ–2θ geometries has been relatively unsuccessful in characterizing cBN thin films. The weakly diffracted X-ray intensity from the thin, low-atomic-number BN films generally results in poor counting statistics. Further complications arise from the peak broadening due to poor crystallinity as well as overlaps with peaks from secondary phases. Improved XRD counting statistics have been obtained by using grazing incidence geometries [55,67,68]. In contrast to X-ray diffraction methods, transmission electron diffraction has the advantage of significantly better counting statistics. Its disadvantages arise because of the relative imprecision in determining the camera constant (typical uncertainty is about 2% without an internal standard) and from the inelastic and multiple scattering processes, which complicate the analysis of diffraction intensities.

Table 3 shows expected diffraction peaks and d-spacings for the cubic phase of BN. The strongest peak is the {111} reflection ($d = 2.09$ Å). Several peaks are very weak (e.g. the {200} reflection ($d = 1.81$ Å)) and are rarely observed.

Although the analysis of diffraction from single-phase cBN is straightforward, the presence of secondary graphitic phases significantly complicates the analysis. Highly crystalline hBN is rarely observed in BN films; instead the turbostratic modification (tBN) is dominant. The interpretation of diffraction patterns from tBN [27,70] is similar in many respects to the interpretation to the turbostratic modification of graphite. Specifically, the general {*hkil*} reflections are absent, and only reflections from the basal, {000*l*}, and prismatic, {*hki*0}, planes remain. The {*hki*0} reflections are often abbreviated as {*hk*} (e.g. {10} and {11}), which emphasizes that the structure retains two-dimensional ordering within the hexagonal sheets but does not have long range three-dimensional order.

Because of the weak bonding between layers, the spacing of the {0002} planes is typically larger in tBN than in the ordered, crystalline material. On the other hand, the {*hk*} reflections, which are representative of the dimensions of the rigid, sp^2-bonded B_3N_3 rings, show less variation in position. For instance, Aita [71] cites studies of sputtered BN films for which the interlayer spacing for the {0002} is 5–15% greater than that for crystalline hBN, although the apparent a-axis dimensions remain

Table 3
Diffraction lines expected for cBN

hkl	d (Å)	I/I_0 (400 keV electrons)	I/I_0 (X-ray) (JCPDS 25-1033) [69]
111	2.09	100	100
200	1.81	0.8	2
220	1.28	49	6
311	1.10	26	3
222	1.04	0.5	1
400	0.90	5	1
331	0.83	8	3
420	0.81	0.4	
422	0.74	9	
333 115	0.70	5	

Table 4
Typical ranges of peak positions observed for tBN

d (Å)	*hkil*
3.50–3.83	0002
2.13–2.22	10
1.23–1.28	11

constant to within ±2%. The typical peak positions for tBN observed in thin films are noted in Table 4. In situations for which tBN is oriented with basal planes parallel to the substrate (i.e. a [0002] out-of-plane texture) (as appears commonly in films grown without ion-irradiation), the (0002) tBN ring will be suppressed in the plan-view transmission electron diffraction pattern leaving only the two-dimensional (10) and (11) rings [72]. The remaining rings are pathologically close to the strong cBN {111} and {220} rings, and, without care, could easily be misidentified as arising from cBN. Fig. 4 shows typical electron diffraction patterns from a tBN film and a mainly cBN film.

Additional secondary phases can also lead to interferences in diffraction analysis. These issues should be of particular concern for situations such as pulsed laser deposition, in which particulates of target material can be incorporated into the film [73]. Crystalline hexagonal boron nitride (i.e. not turbostratic) possesses several strong peaks that are close to cBN reflections. For instance, the positions of the hBN $\{10\bar{1}0\}$ ($d = 2.17$ Å) and $\{10\bar{1}1\}$ ($d = 2.06$ Å) reflections [74] straddle the position of the cBN {111} reflection ($d = 2.09$ Å). Similarly, the strong $\{02\bar{2}1\}$ reflection ($d = 2.11$ Å) from elemental rhombohedral boron [75] is close to the cBN {111} reflection.

Diffraction line broadening is a common measure of relative and absolute grain size [76], and the technique has been applied in several instances to cBN films [50,67,77,78]. However, care must be taken in the interpretation of such broadening. Rickerby et al. [77] noted that the analysis of diffraction broadening underestimated the cBN grain size, relative to that measured by dark-field

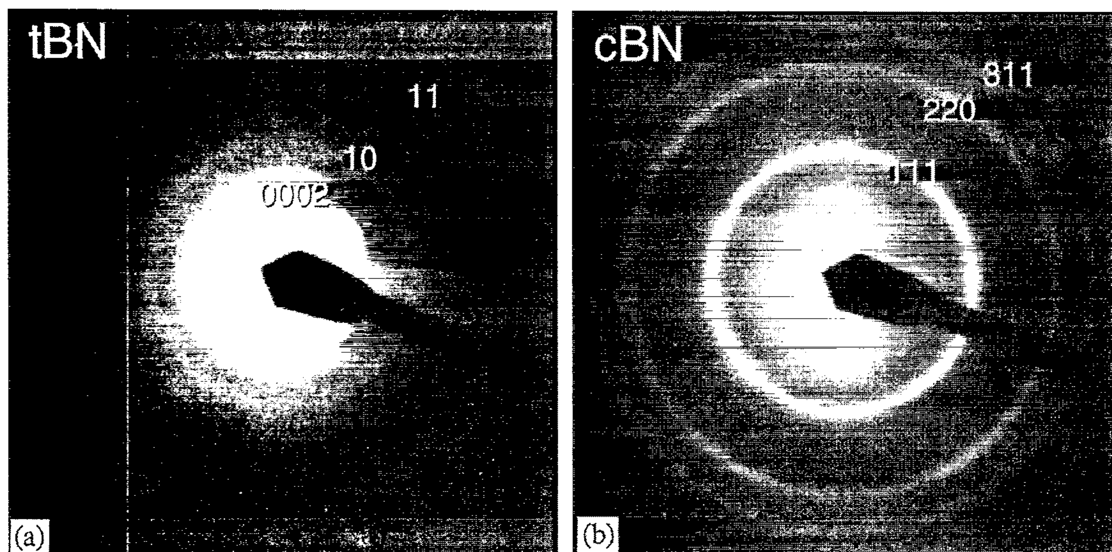

Fig. 4. Electron diffraction patterns from plan-view specimens of (a) a tBN (sp^2-bonded) film and (b) a film with high cBN content. (Note in (b), a weak (0002) tBN ring is present just inside the (111) cBN ring. This arises from residual tBN in the film.)

transmission electron microscopy (TEM), by a factor of approximately 5 and concluded that internal faulting and twinning of the individual grains could explain the discrepancy.

3.3. *Transmission electron microscopy*

TEM has proven very useful for validating phase identification and providing detailed microstructural information about boron nitride films. In this section, we focus primarily on some of the specific details and potential pitfalls in applying such methods to the characterization of BN films. See Section 3.2 for a discussion of electron diffraction applied to characterization of boron nitride films.

3.3.1. *Dark-field TEM*

Dark-field TEM methods are useful for determining the phase distribution and grain size and morphology in cBN films. In the dark-field technique, a small objective aperture is positioned to select a specific diffracted beam, which is used to form the image. For the BN system, segments of the tBN(0002) ring and the cBN(111) ring are commonly used [11,77,79,80]. The regions of high electron intensity in such an image correspond to grains of the phase of interest. Some complications can arise in interpretation because of the overlap of the cBN(111) and the weak tBN(10) rings, particularly if the cBN fraction is small. Additionally, it is important to note that such images do not map out the entire distribution of the phase but rather only those grains that are oriented to diffract into the segment of arc subtended by the objective aperture. This limited sampling can be remedied to some extent by application of conical dark-field methods that are available on some electron microscopes.

3.3.2. *High-resolution transmission electron microscopy*

Because of the nanocrystalline dimensions of the ordered regions of both the sp^2- and sp^3-bonded phases in BN films, high-resolution transmission electron microscopy (HRTEM) has been critical to microstructural studies of boron nitride films. Fringe spacings and angles can aid in phase identification. These can be measured directly from images or in reciprocal space using Fourier transform methods. Measurement accuracy is about 0.1 Å for the nanocrystalline microstructures common in cBN films. For cBN, the most commonly identified fringes correspond to the {111} planes ($d = 2.088$ Å). For the graphitic boron nitride material, the basal plane fringes ($d \approx 3.3$ Å) are easily resolved. Additionally, if graphitic material is oriented along a $\langle 2\bar{1}\bar{1}0 \rangle$-type direction it is often possible to resolve the in-plane periodicities corresponding to the zigzagging chains of alternating boron and nitrogen atoms that run parallel to this direction and which are spaced by 2.17 Å [81,82]. For hBN, the resulting intensity peaks are directly aligned above each other and correspond to $\{10\bar{1}0\}$ fringes; in rBN the peaks are staggered in an A B C... sequence and correspond to $\{10\bar{1}1\}$ fringes. Such contrast has been used to examine the local graphitic BN stacking arrangements in a film grown by ion-assisted pulsed laser deposition (PLD) [83].

Caution must be exercised in the interpretation of HRTEM images. HRTEM contrast is very sensitive to crystal orientation, beam tilt, and the objective lens focus and aberrations [84]. In nanocrystalline specimens such as cBN films, the tilt orientation of individual crystallites is quite difficult to experimentally control. As an example, a tilt rotation as small as 20 mrad about the c axis of hBN is sufficient to obliterate the $\{10\bar{1}0\}$ contrast [82] leaving only the (0002) fringes visible. Additional image artifacts may arise from overlapping crystallites and variations in specimen thickness.[5] For

[5] As discussed in Ref. [85], the presence of HRTEM Moiré fringes from overlapping crystalline regions has in at least one instance been misinterpreted as evidence for epitaxial cBN on silicon.

many geometries, the use of image-simulation programs is a critical aid to the interpretation of HRTEM images.

3.3.3. Electron energy loss spectroscopy

Electron energy loss spectroscopy (EELS) in the transmission electron microscope can provide useful information regarding the bonding character of the boron nitride polymorphs. Issues related to phase identification in boron nitride by EELS have been reviewed recently [86]. In the low-loss regime, the energy of the plasmon peak exhibits a significant shift between hBN ($E_p = 21.5$ eV) and cBN ($E_p = 30.1$ eV), reflecting the large difference in density between the two phases. In the high-energy-loss regime, the near-edge fine structure of the boron and nitrogen K ionization edges can be used to distinguish between sp^2- and sp^3-bonded material as well as to quantify the fraction of sp^2-bonded material on a local scale. For instance, the boron K edge in hBN consists of a sharp peak centered at 191 eV, arising from the $1s–\pi^*$ transition, followed by a broader peak at 198 eV from the $1s–\sigma^*$ transition; in cBN the π^* peak is absent and only a σ^* peak at 196 eV is present. McKenzie et al. [61] used EELS to examine the spatial variation of sp^3-bonding in a cross-sectioned cBN film. Similar analyses have been performed for analyses of amorphous carbon [87] and diamond [88]. EELS in a reflection mode has been used to characterize the near surface regions of cBN-containing films [89]. The near surface regions have been found to be sp^2-bonded, as discussed in Section 6.4.

3.4. Other techniques

As discussed in Section 4.2, film stoichiometry is an important issue, and Auger electron spectroscopy (AES) and X-ray photoelectron spectroscopy (XPS) can provide a chemical analysis of the near surface (top several monolayers) of BN films. The primary limitations of these methods are that (i) the near-surface composition of BN films can differ from the bulk [90], (ii) the use of ion sputtering to clean the surface or depth profile the sample can alter the composition since boron and nitrogen can sputter at different rates [91], and (iii) the electron-beam energies/currents commonly used in AES have been observed to damage BN [92,93]. The latter difficulty can be overcome by using very low electron beam currents [92] and employing special detection techniques (i.e. photon counting).

Wavelength-dispersive X-ray spectroscopy (WDS), performed with a scanning electron microscope (SEM) or an electron probe microanalyzer (EPMA), can be used to measure the stoichiometry of the BN films over a depth of roughly 1 μm (and volume of $\sim 1\ \mu m^3$ [3]). Drawbacks of this technique include (i) beam-induced damage of the sample, and (ii) complications to compositional estimates because of the proximity of the B and N peaks and the shifting of peaks due to matrix effects [72].

Rutherford backscattering spectrometry/elastic recoil detection (RBS/ERD) and neutron depth profiling (NDP) have also provided compositional information on cBN films. These techniques can sample the entire film thickness and can be more accurate than the electron- and photon-based techniques described above. Primary drawbacks are (i) the expense of the needed equipment, (ii) the complicated procedures required to interpret results from BN films [55,94], and (iii) for RBS/ERD, the limited accuracy for cBN films on particular substrates.

Raman spectroscopy has not been widely used to study cBN films, largely because of its inferior sensitivity compared to IR analysis for thin-film analysis. Werninghaus et al. [95] have shown that the Raman peaks of cBN substantially broaden as the crystallite size and distance between defects decreases. This accounts for the difficulty in obtaining well-defined Raman scattering from current cBN films, which have only small, highly defective crystallites. Compared to IR analysis, Raman

analysis is much less influenced by factors such as the film thickness, the optical properties of the substrate, and the sharpness of the film/substrate interface. Therefore, Raman spectroscopy will become more important as the films improve in quality and become thicker. On a cautionary note, there is a 'plasma' line (i.e. a non-lasing emission line) shifted 1057 cm^{-1} from the 488 nm line of argon-ion lasers, a common Raman excitation source [96]. If not properly filtered, this emission line can be misinterpreted as the TO phonon of cBN.

Near-edge X-ray absorption fine-structure spectroscopy (NEXAFS) is sensitive to electronic bonding, and has been used [97–99] to differentiate between BN phases. Distinguishing between *bulk* sp^2-bonded (hBN, rBN) phases was found to be difficult. However, a subtle difference was observed between the *bulk* sp^3-bonded phases, wBN and cBN. NEXAFS measurements on a BN *film* with approximately 15% cBN (via FTIR) showed evidence of both sp^2 and sp^3 bonding. Since NEXAFS is a synchrotron-based technique, its application will be small compared to the widely available technique of FTIR spectroscopy.

Although optical characterization of BN films is useful in itself, care must be taken in using quantities such as the index of refraction to infer phase information. Ellipsometry is commonly used to measure the frequency-dependent real and imaginary parts of the index of refraction, or equivalently, the frequency-dependent real and imaginary parts of the dielectric constant. The (real) refractive index of cBN at visible frequencies is about 2.1 [1,39]. The refractive index of cBN-containing films has been found to be approximately 1.9–2.1 [50,51,100,101]. The optical properties of hBN are highly anisotropic; the refractive indexes parallel and perpendicular to the *c* axis are 2.05 and 1.65, respectively [102]. With increasing substrate bias, Kuhr et al. [51] have indeed observed that the refractive index of tBN produced by plasma-enhanced chemical vapor deposition (CVD) varied from about 2 to 1.65 as the orientation of the *c* axis relative to the substrate changed from parallel to perpendicular. In addition, Dworschak et al. [50] found that the refractive index of tBN increased with B content and that the refractive index of B itself was 2.34. Thus, through either orientational or stoichiometric effects, the refractive index of tBN can be close to that of cBN. Therefore, phase identification based on measurements of refractive index alone is ambiguous.

- The most valuable techniques for phase identification of BN films are infrared spectroscopy, transmission electron diffraction and microscopy, and electron energy loss spectroscopy.
- Since distinguishing cBN from graphitic BN can be difficult, use of complementary phase characterization methods along with stoichiometry analysis is prudent.
- Some possible pitfalls in phase identification: (i) infrared spectroscopy, SiO_x peak near cBN peak; (ii) diffraction methods, possible overlap of tBN and cBN peaks; (iii) HRTEM imaging, overlapping crystallites, thickness variations, specimen tilt; (iv) Raman spectroscopy, artifacts near cBN peak.

4. Factors controlling formation of the cubic phase in BN film synthesis

4.1. Ion bombardment

The recent success in synthesizing cBN films largely results from using energetic particle bombardment (typically via ions) during film growth. In 1987, Inagawa et al. [103] observed that cBN film formation only occurred in a specific range of *ion current (flux)* and *substrate bias* (i.e. *ion energy)* values, as illustrated in Fig. 5. They observed that the process-parameter boundaries, as well as the

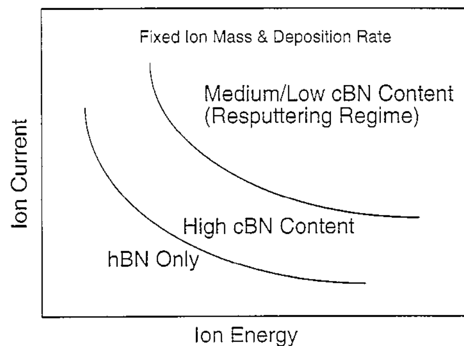

Fig. 5. Schematic diagram showing cBN content as a function of ion current energy at constant ion mass and deposition rate, after Inagawa et al. [103] The transition to low/medium cBN content with increased ion current and energy is now known to result from increased sputtering, which gives a thinner film, and ultimately a no-growth condition.

maximum cBN percentage attained, were influenced by the ratio of Ar^+ to N_2^+ ions (i.e. *ion mass*). In 1990, Ikeda et al. [104] and, in 1991, Yokoyama et al. [59] found a narrow window of *deposition rate and substrate bias* in which cBN formed. With fixed ion mass and deposition rate, Kester and Messier [105], Ikeda [106], and Tanabe et al. [107] observed, in 1992, that cBN formed only for certain values of *ion energy and ion flux*. Thus, there are sharp thresholds for cBN formation in an experimental parameter space of (i) ion mass m, (ii) ion energy E, (iii) ion flux J (ions $cm^{-2} s^{-1}$), and (iv) deposition flux a (atoms $cm^{-2} s^{-1}$). The deposition flux is generally defined as the total flux of boron and nitrogen atoms that arrive at the substrate. However, some researchers refer to the boron flux as the deposition flux. Not all the arriving atoms are incorporated because of ion sputtering. The flux ratio J/a is commonly referred to as the ion-to-atom ratio.

An example of the sensitivity to ion bombardment is given in Fig. 6(a), where a 10% increase in J/a changes the cBN content from essentially zero to ~80%. Based on the ion-assisted physical vapor deposition (PVD) work of Tanabe et al. [107], Kester and Messier [105], Bouchier et al. [109], Ganzetti and Gissler [110], and Mirkarimi et al. [108], Reinke et al. [111–113] refined the parameter–space plot of Inagawa et al. [103]. Fig. 7 displays BN phase formation as functions of ion energy and J/a_B, where a_B is the boron deposition flux. The lower solid line is the sharp boundary between tBN and cBN formation, while the upper solid line is the boundary between cBN and total resputtering (no net film growth). Thinning of the film near the latter boundary emphasizes the graphitic BN interlayer (see Section 6.2), accounting for the decreased cBN content seen in data such as Fig. 6.

In 1992, Kester and Messier (KM) proposed that the sharp threshold for cBN formation could be described by a single momentum-related parameter [105]. Before discussing the KM study further, we provide some background information. The ratio of the ion flux to the atom (deposition) flux, J/a, has a significant effect on many film attributes including film microstructure, stoichiometry, intrinsic stress. Targove and Macleod (TM) derived a parameter meant to describe the momentum transferred from the ions to the film atoms assuming a single, head-on, elastic collision between an ion and a film atom [114]. This momentum-related parameter is:

$$(P/a)_{TM}=\sum_i (J_i/a)\sqrt{2m_i E_i \gamma_i} \quad (2)$$

where m_i is the mass of the ith ionic species, E_i is its mass, and γ_i is the efficiency of kinetic energy transfer in a single, head-on, elastic collision given by:

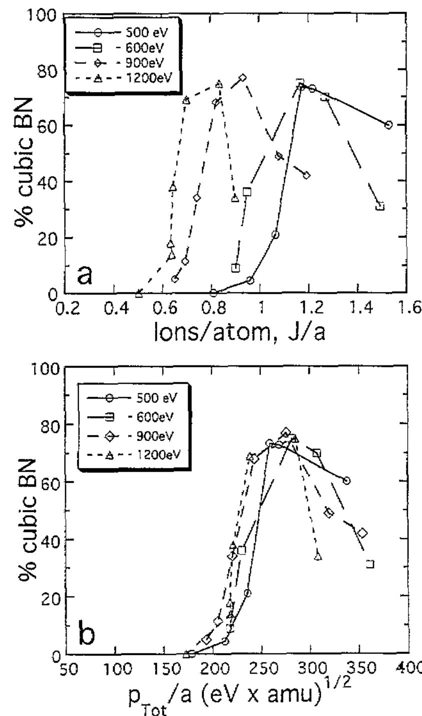

Fig. 6. cBN content as a function of (a) ion per film atom (J/a) and (b) ion momentum per film atom (P_{Tot}/a) for different ion energies and constant ion mass using Eq. (4). The ion-irradiation flux originates from a gas feed of 60% N_2/40% Kr. From Mirkarimi et al. [108].

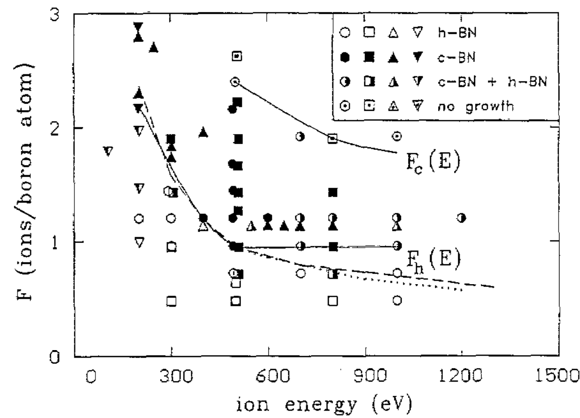

Fig. 7. Formation of BN phases as a function of ion/boron flux and ion energy as compiled by Reinke et al. [113]. cBN forms only between the upper solid line and either the lower solid line or the dotted line. For insufficient relative ion flux (below lower solid line or dotted line), only tBN forms. For too high of an ion flux (above upper solid line), no film growth occurs because of ion sputtering. Note that the tBN/cBN boundary in the lower solid line is fixed at $F=J/a_B=1$ above 500 eV, and is therefore independent of ion energy. Reinke et al. [113] attributed this to the stoichiometry requirement of having sufficient nitrogen ions to react with the evaporated boron atoms to form BN. In contrast, the dotted line represents the data of Mirkarimi et al. [108]. In their technique (ion-assisted pulsed laser deposition), nitrogen comes from the ablation target as well as the ion source. Their results show an $E^{1/2}$ scaling for cBN formation between 500 and 1200 eV.

$$\gamma_i = \frac{4m_i M_{\text{atom}}}{(m_i + M_{\text{atom}})^2} \tag{3}$$

where M_{atom} is the average mass of the film atoms.

Using nitrogen ions and either argon, krypton, or xenon ions, KM [105] measured the cBN content of films grown with varying E and J/a. They found that the sharp threshold for cBN formation could be universally parameterized in terms of $(P/a)_{TM}$. That is, cBN formation occurred above the same critical value of $(P/a)_{TM} \approx 200$ (eV amu) $^{1/2}$ independent of the particular values of J, a, m, and E. For combined bombardment by nitrogen and argon ions, total resputtering occurred above ~ 300 (eV amu) $^{1/2}$. Consistently, several researchers have subsequently found cBN formation to occur near the 200 (eV amu) $^{1/2}$ value[6] [109,110,115]. In studies that varied both E and J/a, Ganzetti and Gissler [110] and Bouchier et al. [109] also found that the cBN-formation threshold scaled as $E^{1/2}$. The KM study was the first to link cBN formation with a 'super-parameter' incorporating all of the factors (J, a, m, and E) observed to have a strong effect on cBN formation.

Varying both m and E in conjunction with J/a, Mirkarimi et al. [108] also confirmed the KM observation that the cBN-formation threshold scaled as $E^{1/2}$. However, they found a different dependence on ion mass. Mirkarimi et al. [108] found that the cBN-formation threshold scaled best with the 'total' momentum of the bombarding ions,

$$(P_{Tot}/a)=\sum_i (J_i/a)\sqrt{2m_iE_i} \tag{4}$$

rather than the momentum transferred in a single, binary collision. For fixed ion mass and variable ion energy and flux, Fig. 6(b) shows that the threshold for cBN formation occurs at essentially the same value of P_{Tot}/a but not the same value of J/a (Fig. 6(a)). The critical P_{Tot}/a value was close to the critical $(P/a)_{TM}$ value of KM. Mirkarimi et al. argued that Eq. (4) is more physically realistic than the single-binary-collision parameter ($(P/a)_{TM}$) since the interaction of a several hundred electronvolt ion does not consist of a single collision, but is instead a complicated cascade involving many separate collisions for which the total ion momentum is ultimately transferred to the film. Furthermore, Mirkarimi et al. [108] noted that the specific momentum parameter used by TM and KM (Eq. (2)) is non-physical since the film-atom mass should replace the ion mass. The physical significance of the momentum scaling is discussed in Section 7.3.

There is evidence that the $(mE)^{1/2}$ scaling breaks down at low ion energies. Ulrich et al. [116] observed that for cBN deposition at $E \approx 140$ eV, 90 eV, and 60 eV, the critical J/a values are approximately 13, 20, and 66, respectively. Similarly, Johansson et al. [117] required $J/a \approx 24$ at $E = 110$ eV. The momentum parameter values calculated from these results are significantly larger than the reasonably consistent values found by Ganzetti and Gissler at $E = 200$ eV and other workers [109,108,118] at $E > 300$ eV. While these studies used Kaufman-type ion sources [109,110,108,118], Ulrich et al. [116] and Johansson et al. [117] used ions generated from sputter-source plasmas. Therefore, some of the difference in momentum values may result from processing and/or measurement differences (see below). For example, while Johansson et al. deposited tBN films at $E \approx 500$ eV and $J/a \approx 3$, either cBN or a sputtered film would be expected for these conditions using a Kaufman source [105,108]. Additional evidence that the $E^{1/2}$ scaling may break down at low ion energies comes from Reinke et al. [111–113,119]. In addition to the data shown in Fig. 7, Reinke and other workers combined results from several ion-assisted PVD [105,107,109,110] and plasma-assisted CVD [50,59,119] studies on one plot. [7] From these two figures, they concluded that for $E < 500$ eV the cBN-formation threshold scaled as the inverse sputter yield (see also Section 7.1), which has an approximate E^1 dependence [111]. Since cBN formation occurs for both PVD and CVD processes in a similar

[6] In general, comparison between different studies is problematic because making accurate, absolute measurements of ion and deposition fluxes is non-trivial.

[7] In the plot, most of the data points, and all of the points between 100–300 eV come from the plasma-assisted CVD study of Kuhr et al. [119].

range of ion-bombardment parameters, Reinke et al. also concluded that the same mechanisms are operable in these two processes (i.e. chemical effects are not dominant in plasma-assisted CVD).

Sené et al. [120] suggest that cBN synthesis is best parameterized by an energy dependence of the form $(E-E_o)^{1/2}$, where the constant E_o is between 100 and 200 eV. The form, derived from simulations of ion–solid collisions, reduces to an approximate $E^{1/2}$ dependence for ion energies greater than 300 eV, and an approximate E^1 dependence (see above) at low ion energies. Unfortunately, most of the literature data below 200 eV comes from plasma-assisted experiments using r.f.-biased substrates [50,59,116,117,119]. The ion flux and energy is derived with some uncertainty from the substrate bias, and the density and temperature of the plasma. The latter are determined by Langmuir-probe measurements, which are problematic when the probe is being coated with an insulating film such as BN or is in the presence of a magnetic field. Clearly, additional and more accurate data at lower ion energies are needed to determine whether other functional forms indeed are an improvement upon the simple momentum scaling.

If ion-induced atomic displacements are important to cBN formation (see Section 7), then, as suggested by Kidner et al. [78], cBN synthesis should not be possible at energies near or below the displacement energy of atoms in BN (several tens of electronvolts). Several groups have deposited predominantly cBN films at ion energies near or below 100 eV [59,78,117,119,121]. However, there is not yet convincing evidence for cBN synthesis below $E \approx 50$ eV. From a study of the ion-energy dependence, Kidner et al. [78] proposed an ion-energy threshold of ~ 100 eV for cBN synthesis. However, more recently the same group [66,121] synthesized cBN at even lower ion energies by using higher ion-to-atom (J/a) values.

Evidence also supports the notion that the initiation and growth processes in cBN synthesis are separate. Recently, McKenzie et al. [122] and Hahn et al. [123] reported that the ion energy necessary to first form (nucleate) cBN is higher than the ion energy needed to subsequently grow cBN. That is, once a cBN layer was formed, cBN growth could continue for a markedly lower ion energy. Hahn et al. [123] also reported that a larger ion momentum per deposited atom is necessary to initiate cBN formation than to subsequently grow cBN. The implications of these observations are discussed in Section 7.5.

In addition to E, m, and J/a, several deposition system-specific parameters affect cBN formation. One such parameter is the angle of incidence, measured from the surface normal, between the impinging ions and the film. Using 500 eV ions, Sueda et al. [124] varied J/a and varied the angle of incidence from normal to glancing. They found that predominantly cBN films could be synthesized at all the ion angles, at roughly *similar* J/a values. The window of J/a values for cBN formation narrowed, however, with increasing ion angle. Since the upper bound of the cBN-formation window is the threshold for total resputtering (see Fig. 7), and TRIM simulations indicate that the sputter yield for typical growth conditions increases for increasing angles up to about 80° [125,126], this window narrowing is indeed expected [124]. In contrast, Bouchier et al. [109] reported that the threshold J/a value for cBN formation *decreased* by almost 40% as the incidence angle of 300 eV ions increased from 15° to 45°. However, the support for this conclusion consisted of only three data points and further investigation is desirable. Mirkarimi et al. [127] showed that the temperature threshold for cBN formation (see Section 4.3) decreased somewhat when the incidence angle increased from 60° to 80°. That the thresholds in J/a and temperature are functions of incidence angle may be related to the spatial distribution of ion-induced defects, which has been suggested to affect cBN formation [108]. The maximum, localized defect density becomes larger and moves closer to the surface as the incidence angle increases [125,126].

In summary, ion bombardment plays a key role in cBN film synthesis. The models proposed to explain the mechanism of cBN formation through ion bombardment will be described and critiqued in Section 7.

4.2. Stoichiometry effects

From analysis of their own work and an examination of the literature [104,107,118,128–131], Hackenberger et al. [65] concluded that films with high cBN content tended to have B/N ratios close to unity. More recent work has also supported this observation [50,51,94], which is not surprising since cBN is a line compound. Although the B/N ratio needs to be near unity for the BN film to be *predominantly cubic*, cBN has been observed [132] in mostly tBN films with B/N ratios differing significantly from unity. Whether the B/N ratio is homogeneous throughout these films or is locally stoichiometric in the vicinity of the cBN grains remains to be determined. This knowledge is necessary to assess the degree to which local compositional fluctuations control cBN formation. Regardless of the local effects, it is clear that overall stoichiometry is required to obtain nearly phase-pure films.

4.3. Temperature effects

Several studies have investigated the temperature dependence of cBN formation in detail [55,105,107,127,133,28]. Dworschak et al. [50] have also studied temperature effects in a CVD process where hydrogen incorporation is an additional concern. These studies find that cBN films can be grown over a wide range of temperatures, in contrast to the rather narrow range of ion-to-atom ratios for which growth is possible. For example, Friedmann et al. [55] reported high cBN content in films grown at temperatures from about 100 °C to over 800 °C. Substrate temperatures of several hundred degrees Celsius are commonly used. That cBN can be grown at these relatively low temperatures has much appeal, particularly in contrast to the 1000 °C-type temperatures used for making diamond by CVD processes [4]. While 'room-temperature' growth has been reported [134,135], the actual substrate temperature is probably above room temperature because of heating from energetic particle bombardment.

For fixed deposition conditions and film thickness, as the temperature is *increased* beyond some 'optimal' temperature (typically 400–500 °C), the volume-averaged cBN content decreases somewhat from the increased thickness of the sp^2-bonded BN layer (see below). As the substrate temperature is *reduced*, the ability to make cBN is lost entirely at some process-specific temperature. For example, Tanabe et al. [107] found a threshold temperature below which only tBN, not cBN, was produced. The threshold temperature increased from about 90 °C to about 230 °C with increasing ion-to-atom ratio. The following has been reported for a fixed ion-to-atom ratio: Kester et al. [133] found that temperatures $>$200–300 °C were required to make single-phase cBN; Friedmann et al. [55] could readily produce cBN on silicon for substrate temperature $\gtrsim 100$ °C, but not at lower temperatures, consistent with more recent results by Hofsäss et al. [101]. For all ion-to-atom ratios up to complete resputtering, Mirkarimi et al. [127] could grow predominantly cBN films at ~ 130 °C, but could not synthesize cBN below ~ 100 °C, indicating that the inability to grow cBN below the threshold temperature is not because of a particular ion-to-atom ratio.

The existence of this low-temperature threshold is unexpected both from a thermodynamic perspective and in light of the large amount of ion energy dissipated during film growth. While recent work (see Section 2.2) has questioned whether hBN is the equilibrium phase under ambient conditions, there is agreement that the slope of the cBN/hBN boundary ($\partial P/\partial T$) is positive. This implies that at constant pressure under equilibrium conditions, a reduction in temperature should favor the growth of

cBN, behavior opposite to that of the observed temperature threshold. While the temperature of the substrate (typically a few hundred degrees Celsius) is low compared to the melting points of hBN and cBN, the ion energies per film atom required for cBN formation are sufficient to displace each film atom from its binding site on the order of ten times (see Section 7). This very large energy input is probably why cBN synthesis is relatively insensitive to substrate temperature once the threshold temperature is exceeded. The temperature dependence for making sp^3-bonded BN is also different from the temperature dependence for synthesizing sp^3-bonded amorphous carbon. Apparently there is not a temperature below which sp^3-bonded carbon cannot be formed [136]. McCarty et al. [28] have shown that cBN can be grown below the threshold temperature on cBN which itself had been grown above the threshold temperature. They suggested that cBN nucleation requires a higher temperature than cBN growth.

Kidner et al. [78] and Taylor and Clarke [121] have used low ion energies and deposition rates to synthesize high cBN content films at very high temperatures (850–1200 °C). Taylor and Clarke [121] and Mirkarimi et al. [137] report that this route can allow for growth of thick cBN films since the residual stress is reduced, as discussed further in Section 9.1.

The microstructure of the BN films clearly varies with substrate temperature. Using cross-sectional HRTEM and IR analysis, Kester at al. [133] observed that the thickness of the interfacial sp^2-bonded layer increased with increasing substrate temperature. This effect could be compensated for by increasing the ion-to-atom ratio. The thickening interfacial layer accounts for the falloff in cBN content with increasing substrate temperature that is observed in constant thickness experiments. The crystallinity of the cBN worsens as the growth temperature decreases, as evidenced by the increasing width of the TO phonon in IR spectroscopy [55]. McCarty et al. [28] have studied how the sp^2-bonded material accompanying cBN formation changes with temperature. They showed that the ordering of the sp^2-bonded basal planes increased with increasing substrate temperature.

In summary, cBN films can be grown at relatively low substrate temperatures. While cBN growth is not achieved below some process-specific temperature, above this temperature the cBN content is not a sensitive function of temperature. While possibly making the initial nucleation of cBN more difficult, high-temperature growth holds promise for reducing intrinsic stress and improving crystallinity.

4.4. Substrate effects

While the vast majority of cBN film studies have employed silicon substrates, as shown in Table 5, several other substrates have also been used. Films with a high cBN fraction can be deposited on a wide variety of substrates. As noted in Section 3.1, the relative IR response will be different for metallic and non-metallic substrates, so quantitative comparisons are complicated. This aside, the literature indicates that the highest cBN-content films form on hard, covalent substrates such as Si, SiC, and diamond. Mirkarimi et al. [127] observed that BN films deposited on soft metal substrates (Al, Ag) had a much lower cBN content than films on harder metal substrates (Nb, Ta, Ni), suggesting that substrate strength plays a role in cBN formation. There is support for this conclusion in the literature, although the data from soft substrates are sparse. The mechanistic implications of this work will be discussed in Section 7.3.

There are only a few reports where the cBN content on insulating substrates has been quantified. For instance, although cBN growth on sapphire has been reported [146], Mirkarimi et al. [127] had difficulty obtaining cBN on insulators and suggested that substrate charging could be causing a reduction in ion-current density. The use of an r.f. substrate bias would be one way to overcome this obstacle. As discussed in Section 9.1, the substrate may also influence film adhesion.

Table 5
Summary of cBN film growth on non-Si substrates

Substrate	Reference	Charac. technique	~ cBN content [a]
a-C/Si	[56]	FTIR	Very high
Al/Si	[138]	XRD	Low?
Al	[139]	FTIR	Low/med.?
Al	[56]	FTIR	Low
Ag	[56]	FTIR	Low
Au	[56]	FTIR	Medium
B/Si	[140]	FTIR	Very high
Cu	[133,139]	FTIR	None
Cu	[56]	FTIR	Medium
Diamond	[141]	FTIR	High
Diamond	[133]	FTIR	Very high
Mo	[139]	FTIR	High
Mo	[56]	FTIR	High
Ni/Si	[138]	XRD	High?
Ni	[104]	FTIR	Medium
Ni	[56,133]	FTIR	High
Ni	[142]	XRD	Very high?
Nb	[56]	FTIR	High
Pt/Al_2O_3	[56]	FTIR	Medium
β-SiC/Si	[127]	FTIR	Very high
Steel	[61,104,139,143]	FTIR	High
Ta	[56]	FTIR	High
TiN/WC–Co	[144]	XRD	High?
TiN/WC–Co	[104]	FTIR	High
TiN/MgO	[56]	FTIR	High/very high
WC	[145]	FTIR	Very high?
WC–Co	[104,143]	FTIR	High

Very high, >85% cBN; high, ~60–85% cBN; medium, ~35–60% cBN; low, ~5–35% cBN; none, <5% cBN.
[a] "?" denotes that quantitative estimates are difficult since either XRD was used, or IR spectroscopy was used but few details are given.

Ikeda et al. [104] observed that *surface roughness* can influence cBN film formation. Growth on a 'mirror-like' silicon surface (max. roughness <0.01 μm) gave a much higher cBN content than growth on a 'rough' (max. roughness <0.4 μm) silicon surface [104]. A possible explanation is that the roughness shadows small areas of the film from ion irradiation.

- Intense ion bombardment is required to form cBN films.
- For ion energies >200–300 eV, cBN film synthesis can be parameterized in terms of the ion momentum per depositing atom. At lower ion energies, other parameterizations may be more accurate.
- More energetic conditions and a higher substrate temperature are required to initially form (nucleate) than to subsequently grow cBN.
- Films with high cBN content are nearly stoichiometric.
- There is a sharp, low-temperature threshold below which cBN does not form. Above this temperature, cBN content is insensitive to temperature.
- While most growth has been on silicon substrates, films with high cBN content have been obtained on other hard ceramics and metals.

5. Survey of cubic BN film synthesis techniques

In this section we categorize the various studies by the technique used to provide the deposition flux. As noted in Section 4.1, energetic-particle bombardment during film growth is necessary to synthesize high cBN-content films. Thus the processes differ primarily in the sources of B and N and how the ions are generated and transported to the substrate. In Fig. 8, we show a simplified schematic illustration of the two basic processes: ion-assisted deposition and plasma-assisted deposition.

5.1. Electron-beam evaporation/ion plating

Ion-assisted electron-beam evaporation, sometimes referred to as 'ion plating,' was one of the first techniques used in early attempts at cBN synthesis. In 1987, Inagawa et al. [103] showed that this technique could deposit nearly-phase pure cBN films. On one of the samples, the FTIR spectrum shows essentially the single peak of cBN. Nearly phase-pure cBN films have since been synthesized via electron-beam evaporation by a number of groups [12,61,65,104–106,109,122,124,130, 133,143,146–149]. In several of these studies [12,105,106,124,130,133,148], ions from sources, such as a Kaufman-type sources, bombarded the growing film with little or no bias applied directly to the substrate. The other processes [61,103,104,143,146,147] involve striking a plasma discharge and extracting and accelerating ions to the biased substrate (radio frequency (r.f.) usually). There are also hybrid processes. For example, Lu et al. [150] recently grew films of predominantly cBN using a modified Kaufman-like source that generated energetic *neutrals* instead of ions.

5.2. Ion-assisted pulsed laser deposition

Synthesis of polycrystalline cBN films using *ion-assisted* pulsed laser deposition (PLD) is well established. In 1990, Mineta et al. [151] synthesized cBN films by combining a deposition flux generated by ablating a hBN target with a *continuous* CO_2 laser with an ion flux from a Kaufman source. Using pulsed excimer lasers but otherwise similar experimental configurations, other workers [55,79,108,127,152] since then have obtained films with high cBN percentages (of $\geq 85\%$). Advantages of using ion-assisted PLD for cBN deposition include: (i) separate ion and deposition sources, which permits independent control of the deposition rate, ion flux, etc.; and (ii) the simplicity of the technique, in which multicomponent (i.e. BN) targets can be used. Disadvantages of PLD include limited potential for industrial scale-up and particle incorporation into the film. The particles, which

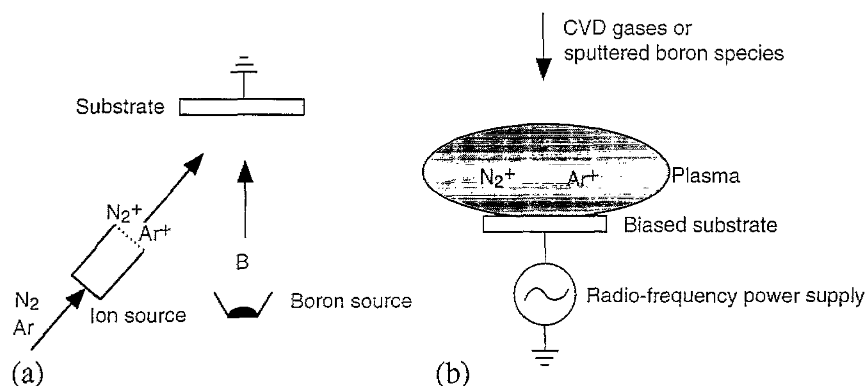

Fig. 8. Simplified schematic illustrations of two basic techniques for cBN deposition. In ion-assisted deposition (a), an ion flux from an ion source is combined with a 'deposition' flux from a source such as a boron evaporator. In plasma-assisted deposition (b), the substrate is typically r.f. biased and ions from a plasma discharge are accelerated toward the substrate.

originate from the target, can be minimized by using dense (pyrolytic) BN targets [73], and mechanical choppers [153], which take advantage of the much higher velocity of the ablated atomic species relative to the particles.

5.3. Sputtering

Early efforts to use r.f. magnetron sputtering to deposit cBN films were largely unsuccessful [71,154,155]. However, there are now numerous studies reporting high-cBN-content films using this technique [60,72,78,110,117,121,128,129,137,139,156,157]. This success largely results from techniques that enhance ion bombardment during film growth. Merely applying a negative bias voltage to the sample has been shown in several cases to produce cBN films [60,72,157]. The use of magnetic fields to extend the sputter-source plasma out toward the sample can increase the ion flux (J) on the film, and hence allow for a higher deposition rate (a). Both unbalanced magnetron sputter sources [58,117], as well as conventional magnetron sources combined with external magnets/coils [128,139,156,158] have been used to extend the plasma. The necessary ion bombardment can also be provided via a Kaufman-type ion source [110] or with an electron cyclotron resonance ion source coupled with a sample bias [78]. Tanabe et al. [107,159] obtained predominantly cBN films by ion-beam sputtering boron targets. Unlike the results from magnetron sputtering studies, however, no cBN was formed when a hBN target was used.

Sputtering is commonly used in industry for depositing hard coatings. In part, the sputtering studies have addressed solving the practical problems needed for industrial implementation. Radio-frequency magnetron sputtering, needed when insulating targets such as hBN are used, generally has a lower deposition rate than d.c. sputtering. Lüthje et al. [139] and other workers [117,158,160,161] have sputtered a B_4C target (with N_2 added to the ambient) to deposit BN films with a large cBN fraction. Since B_4C (resistivity $< 10^2\ \Omega$ cm) is more conductive than hBN (resistivity $> 10^{10}\ \Omega$ cm), it has potential for use in high-rate d.c. sputtering. Johansson et al. [117] used d.c. sputtering to deposit films with high cBN content. Surprisingly the cBN films have a low carbon concentration of only ~ 5 at.%, even though the target has ~ 20 at.% carbon. Possible explanations for this effect have been suggested [117].

Boron is a potential target material for d.c. sputtering since it becomes sufficiently conductive above 800 °C. In fact, Hahn et al. [157] have d.c.-sputtered hot boron targets and obtained films with high cBN content. Compared to r.f. sputtering, however, they found that the ion flux on the substrate was a factor of three lower with d.c. sputtering. This suggests that cBN growth would occur at a *lower* rate for d.c. sputtering. Also, Schütze et al. [158] were able to obtain films with a much higher cBN fraction using r.f. versus d.c. sputtering, possibly also because of differences in the ion flux. Thus d.c. sputtering may not result in the hoped-for higher cBN deposition rates.

Encouragingly, ion-assisted sputtering yields cBN films as good as any of the other techniques and is easily amenable to industrial scale-up. One disadvantage of sputtering (both d.c. and r.f.) for research studies is the inherent coupling of the ion flux (J) and deposition flux (a), which makes it more difficult to independently vary, control, and measure these important parameters.

5.4. Plasma-assisted CVD

Plasma-assisted chemical vapor deposition (PACVD) was one of the first techniques used to deposit predominantly cBN films [140,162–165]. Ions from either a microwave (2.45 GHz) or an r.f. (13.56 MHz) plasma are extracted and accelerated to the biased substrate. A variety of source gases have been used, and the following source/carrier gas combinations have been demonstrated to

produce predominantly cBN films: B_2H_6 in N_2 [50,68,140,162,163,166,167] or NH_3 [168]; BH_3–NH_3 in H_2 [164]; $NaBH_4$ in NH_3 [169]; $HBN(CH_3)_3$ in N_2 [119]; and $B_3H_3N_3(CH_3)_3$ in N_2 [93]. Unfortunately the most commonly used source gas, diborane (B_2H_6), is both toxic and explosive. This prompted Weber et al. [93] to use less toxic and non-explosive *N*-trimethylborazine ($B_3H_3N_3(CH_3)_3$). One drawback of this source gas is that substrate temperatures of > 750 °C appear to be necessary to produce cBN films, while the diborane process can be used at much lower temperatures, typically ≤400 °C [50,59,140,163,167]. Interestingly, these latter substrate temperatures are not much higher than those reported by researchers using PVD techniques. CVD processes usually have higher substrate temperatures than PVD processes because they rely on thermally driven chemical reactions to crack the source gases, whereas in PACVD the plasma serves that purpose.

Like sputtering, CVD is a practical deposition technique that is amenable to industrial scale-up. CVD is generally inexpensive and can coat irregular shapes better than the PVD techniques. The current disadvantages in using PACVD for cBN film synthesis include: (i) more variables and possible contaminants than PVD techniques, (ii) lower cBN-content films than PVD techniques [50,51,59,68,93,119,163,164,166–168,170,171,172,173], and (iii) the use of hazardous source gases such as diborane.

5.5. Other energetic techniques

Hofsäss and coworkers [101,132] used mass-separated ion-beam deposition (MSIBD) to synthesize films with high cBN content. In this unique process, singly ionized B^+ and N^+ provide the ion irradiation *and* the deposition flux, i.e. no other ions (such as Ar^+, B^{++}, or N_2^+) and no neutral atoms (B°, N°) are involved. The technique has the advantage of allowing for precise, independent control of the ion-bombardment parameters (flux, energy) of all species and leaves no unwanted residual inert gas in the films. That this technique yielded nearly phase-pure cBN films without inert-gas ions demonstrates that inert gas incorporation is not a necessary factor in cBN formation [174,175]. Since both the depositing species are energetic ions, the 'ion/atom' ratio is fixed at one or two, depending on the definition (see Section 4.1). For cBN formation, sharp threshold values of 125 eV for the ion energy and 150 °C for the substrate temperature were found (see Fig. 9) [101]. The energy threshold was interpreted as the minimum energy to enable complete rearrangement of the atoms within the thermal-spike volume (see Section 7.2). Because of reduced film sputtering, the cBN-formation window extended from about 125 to 1000 eV, which is wider than the typical windows of

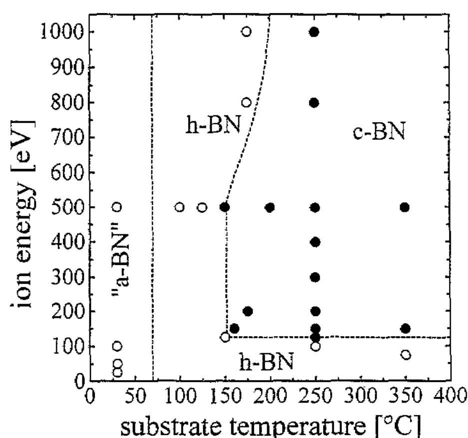

Fig. 9. Formation of cBN grown by mass-separated ion-beam deposition (MSIBD) as function of ion energy and temperature. From Hofsäss et al. [101]

other techniques. The energy threshold of 125 eV corresponds to an ion momentum per incident boron atom ('ion') of about 115 (eV amu) $^{1/2}$, about half the threshold value found in ion-assisted deposition studies at higher ion energies (see Section 4.1). For energies near 125 eV, MSIBD can synthesize cBN with somewhat fewer (see, for example, Fig. 7) to considerably fewer [116,117] ions per incident boron (also see the discussion of Section 4.1) than ion- or plasma-assisted deposition.

Berns and Cappelli have grown cBN films using a low-density supersonic plasma jet, fed by BCl_3 and N_2, impinging on a substrate biased between -60 and -90 V [176].

Cathodic arc evaporation is a process capable of high deposition rates in which a large fraction of the evaporated atoms are ionized. Unfortunately, the technique requires an electrically conductive target and boron and boron nitride are insulators at room temperature. However, boron does become conductive at high temperatures (> 800 °C). Krannich et al. [177] and Richter et al. [178] have used heated boron sources to deposit nearly phase-pure cBN films by cathodic arc evaporation.

5.6. Non-energetic techniques

In contrast to the highly energetic deposition processes described above, cBN synthesis by processes that are considerably less energetic or even thermal has been reported. Examples include hot-filament-assisted evaporation of boron [179,180], metal–organic CVD *without* the use of a plasma [181], and 'non-assisted' PLD [182–188] (i.e. without a supplemental source of energetic ions). (The primary supporting evidence in one of these reports [184] was later [49] determined to be an artifact of the TEM analysis.[8])

Generally, in the reports of cBN synthesis by thermal or non-highly energetic processes, either phase characterization was performed by an insufficient number of complementary techniques (see Section 3) or the characterization data contain irregularities or inconsistencies. Perhaps more importantly, the non-highly energetic approaches claiming cBN synthesis have not been readily reproduced in other laboratories. This is in sharp contrast to the CVD synthesis of diamond, which was widely and easily achieved worldwide following early literature reports [189]. For example, unlike cBN synthesis by ion-assisted PLD (Section 5.2), reproducible synthesis of cBN using non-assisted PLD has not been achieved despite a number of thorough studies [49,188,190,191]. (Conventional PLD is somewhat unique in that the ablated species can have energies of several tens of electronvolts. Therefore the technique is neither a thermal process nor a 'highly-energetic' process. Narayan et al. [192] have suggested that the energetic PLD species promote cBN stabilization compared with thermal techniques such as electron-beam evaporation. However, since cBN synthesis typically requires ion energies of hundreds of eV per film atom (see Section 4.1), it is doubtful whether the PLD process significantly enhances the phase stability of cBN.) We conclude that, at this time, cBN-film synthesis has not been reproducibly achieved through non-highly energetic processes.

Insight into the difficulty of 'chemical/thermal' synthesis of cBN comes from Bohr et al. [33]. They examined why diamond can be readily synthesized by various thermal CVD processes (i.e. without ion assistance), unlike cBN. They invoke two empirical chemical rules. The first is the Ostwald rule, which states that if energy is withdrawn from a system with several energy states, the system will pass through all intermediate metastable states instead of going to the ground state directly. The second is the Ostwald–Volmer rule, which states that the less-dense phase is formed (nucleated) first. In the carbon system, the Ostwald–Volmer rule favors graphite (the less-dense phase) while the Ostwald rule favors diamond formation (the metastable phase). Atomic hydrogen can suppress graphite formation and hence suppress the Ostwald–Volmer rule, allowing the Ostwald rule to dominate and

[8] Cu contaminants were introduced during TEM specimen preparation.

diamond to nucleate/grow. Bohr et al. [33] note that if cBN is the thermodynamically stable phase near ambient (see Section 2.2), then both rules favor hBN formation since hBN is both the less-dense and the metastable phase.

- Nearly-phase pure cBN films can be synthesized by a variety of *highly energetic* deposition techniques.
- Non-highly energetic processes of cBN film growth are not readily reproducible.

6. Microstructure of cBN films

Cubic BN films grow with a unique microstructure consisting of layers of sp^2- and sp^3-bonded material. Using infrared analysis combined with ion-beam sputtering, Inagawa et al. [193] showed in 1989 that a layer of sp^2-bonded BN formed before cBN. Halverson et al. [194] noted a variation in cBN yield with film thickness and speculated that the cBN nucleation was thickness or stress dependent. McKenzie et al. [11] used EELS to characterize a BN film grown by an ion-plating process and noted that sp^2-bonded material formed close to the interface whereas sp^3-bonded material formed further up in the film. Kester et al. [12], using FTIR and HRTEM, identified three distinct layers in the microstructural evolution: a 20 Å thick layer, which was attributed to amorphous boron nitride at the substrate interface; a 20–50 Å thick layer of strongly oriented graphitic BN; and a top layer of polycrystalline cBN. The essential aspects of this layered microstructural evolution, which is shown schematically in Fig. 10 and in TEM images in Figs. 11 and 12, have been subsequently observed by a number of

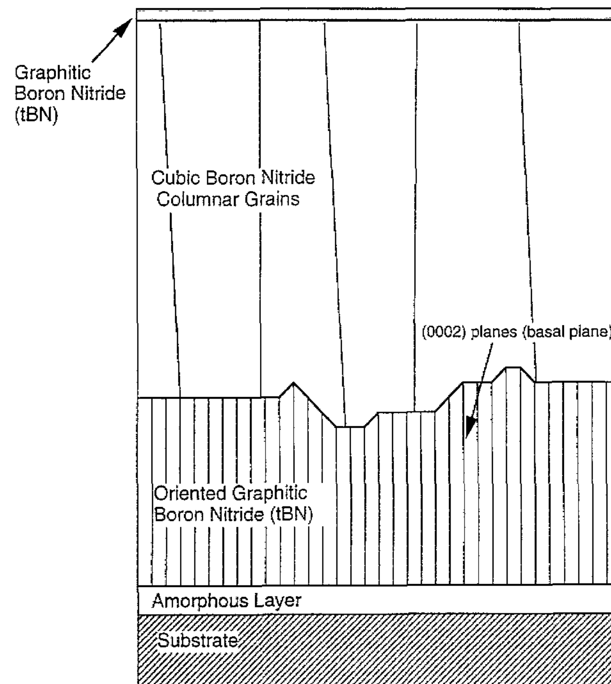

Fig. 10. Schematic diagram summarizing microstructural features of cBN films. A layered structure is typically found, with a layer of oriented tBN forming before the cBN crystallites form. An amorphous layer is commonly observed between the substrate and the tBN layer. The cBN layer is capped by an sp^2-bonded BN layer.

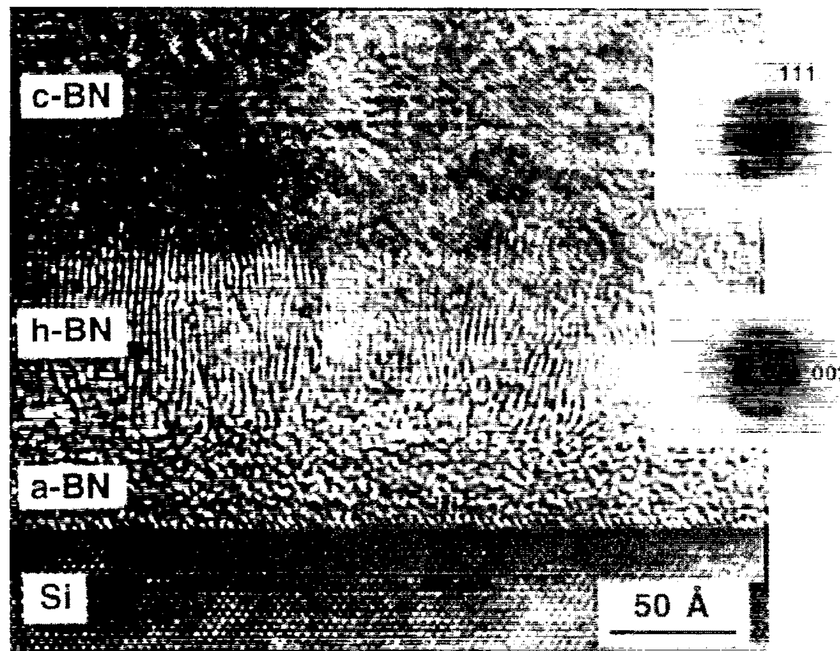

Fig. 11. HRTEM image of a cBN film in cross-section showing the distinct layered structure consisting of an amorphous layer, a strongly oriented graphitic BN layer, and a polycrystalline cBN layer. From Kester et al. [195].

groups using a variety of growth techniques [55,80,160]. The detailed aspects of the microstructure in each of the layers is considered next.

6.1. Amorphous BN layer

The question of whether the initial amorphous layer is an intrinsic and necessary stage of the microstructural evolution remains open. Although it is often described as amorphous boron nitride (aBN), as yet there has been no analytical determination of the chemical identity of this layer. Kester et al. [195], borrowing from notions developed to describe amorphous carbon deposition, suggest that growth of the amorphous layer is controlled by the conduction of heat into the substrate: as the layer thickens it limits the transport of heat into the substrate allowing the next layers of material to form in a more ordered state. Alternatively, Hofsäss et al. [132] explain the amorphous material as an ion-mixing layer and note that the layer thickness is comparable to the ion range. Consistent with this explanation, Hofsäss et al. [196] found that textured tBN, but no amorphous material, was produced between two cBN layers. In addition, Cardinale et al. [197] have presented thermodynamic arguments suggesting that a mixture of boron and silicon oxides may form at the interface following the permeation of water vapor through the film.

6.2. Graphitic BN layer

Graphitic, turbostratic boron nitride (tBN) coatings grown in the absence of a plasma or substrate bias generally are either completely randomly oriented or, given sufficient atomic mobility at elevated temperatures, grow with the basal planes aligned to the plane of the substrate. For a flat substrate, this results in an out-of-plane [0002] texture (see Fig. 13(a)). However, application of a plasma or ion-irradiation leads to a striking change in crystallographic texture. As was first noted by McKenzie et al. [11], the graphitic BN in films grown by ion-assisted deposition exhibits a strong preferred orientation

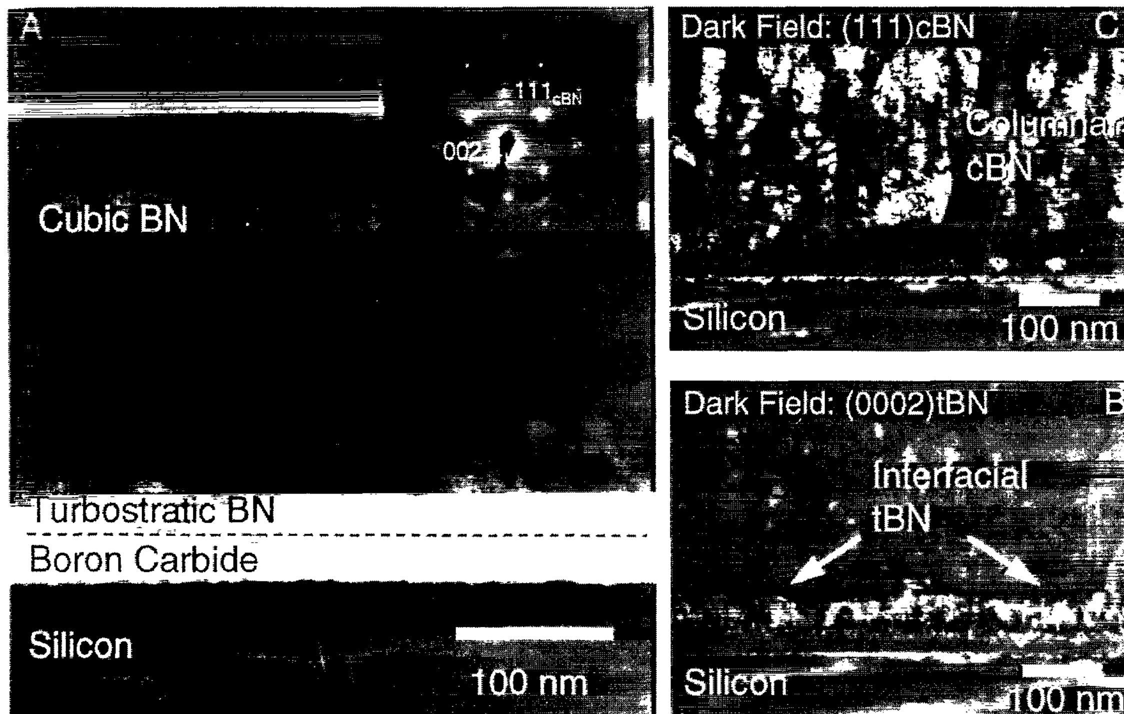

Fig. 12. TEM image of a cBN film in cross-section. (a). Bright-field image with an electron diffraction insert showing a boron carbide layer deposited on the silicon substrate as an adhesion aid, the tBN layer, and finally the cBN layer. Crystallographic texture in both the cBN and tBN layers results in non-uniformities in the electron diffraction rings. (b). Dark-field TEM image obtained from the tBN (0002) diffraction ring showing the tBN layer (bright region) below the cBN. (c). Dark-field TEM image obtained from the cBN (111) diffraction ring showing columnar cBN grains extending from the tBN layer to the top of the film. From Mirkarimi et al. [137].

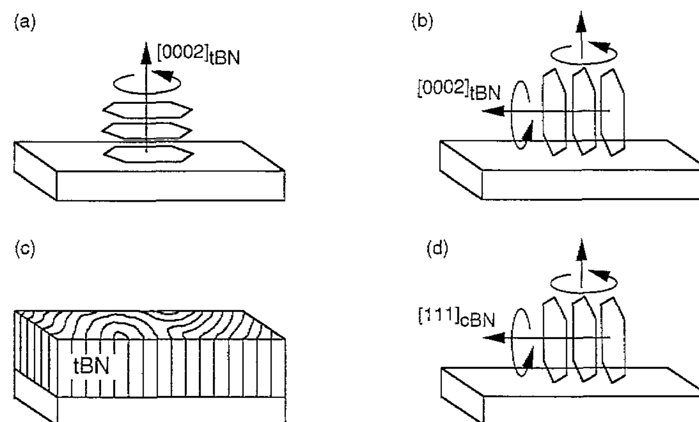

Fig. 13. Schematics showing (a) [0002] out-of-plane orientation for tBN, (b) [0002] in-plane orientation for tBN, (c) 3D view of basal-plane orientation in tBN (after McCulloch et al. [198]), and (d) [111] in-plane orientation for cBN.

with the [0002] direction lying in the plane of the film (i.e. the basal planes are perpendicular to the substrate) (Fig. 13(b) and 13(c)). We will refer to this as a [0002] in-plane texture. Several aspects of this texture are important to clarify. First, the orientation of the [0002] directions about the film normal are random. Second, the graphitic layers are rotated randomly about the [0002] directions. That is, there appears to be no preferred out-of-plane direction.

In 1991, McKenzie and coworkers proposed that the [0002] in-plane texture of the tBN layer results from ion-induced compressive stress [11,61,199]. They considered the anisotropic elastic properties of a hBN crystal in a state of biaxial compressive stress, such as that imposed on a film by a substrate. The Gibbs energy calculated for the elastically strained crystal was smaller if the basal planes were perpendicular rather than parallel to the stress plane. Therefore, they proposed that of the two orientations, the texture with the *c* axis in the stress plane is favored because of its lower Gibbs free energy. Cardinale et al. [200] extended this analysis by examining all possible orientations of the stress plane relative to the crystallographic directions. They found that the configuration with lowest Gibbs energy is not that with the *c*-axis oriented in the plane of the stress, but rather is that with the basal planes tilted roughly 45° from the substrate. (This angle corresponds to direction of highest compliance in the crystal [26].) Cardinale et al. concluded that the experimentally observed texture is not satisfactorily explained by elastic-strain-energy arguments, and instead proposed that the texture is produced when the graphitic BN *plastically* deforms to relieve the ion-induced compressive stress [200]. This mechanism has been discussed in detail by McCarty and Medlin [201]. They showed that the well-established modes of plastic deformation in graphitic materials, basal-plane slip and kinking, would produce a rotation of the *c* axis towards the plane of biaxial compressive stress. Once the *c* axis has rotated to lie in the plane of the substrate, further deformation by basal-plane slip or kinking cannot occur. The stress level should rise if further strain (through additional ion irradiation, for example) is introduced into the material. In terms of the stress-driven models of cBN formation (Section 7.3), at least, their proposal provides an explanation of why an oriented tBN layer is consistently observed in cBN films—only in tBN with a [0002] in-plane texture can sufficient stress be generated to nucleate cBN.

6.3. cBN layer

The grain sizes observed in cBN films are quite small, ranging in diameter from a few nanometers to at most about 100 nm [11,77,79,80,146,166,202]. Grains frequently grow in a columnar morphology starting from the point of nucleation at the top of the graphitic layer and elongating towards the surface of the film (see Fig. 12) [79,203]. Kester et al. [12] suggested that once nucleated, the cBN grows as a single phase. However, subsequent work has suggested that graphitic BN may exist between the individual cBN grains [204]. Whether this is universally true of the grain boundaries in cBN films is unclear.

As shown in Fig. 14, cBN grains exhibit high twin and stacking fault densities. Rickerby et al. [77] noted that cBN crystallites, observed with dark-field TEM, appeared faulted and, in order to explain the width of excessively broadened X-ray diffraction peaks, postulated that the grains were subdivided into narrow twin lamellae. HRTEM observations have confirmed the presence of narrowly spaced {111} twins and stacking faults separated by only a few lattice planes in thin film cBN grains [80,205]. Medlin et al. [80] observed groups of parallel twin lamellae and stacking faults on only one set of parallel {111} planes within any given cBN grain. However, subsequent TEM studies on relatively large-grained cBN films [202] have demonstrated the presence of intersecting twin lamellae on multiple sets of {111} planes.

As with the graphitic layer, the cubic phase exhibits preferential crystallographic orientation. Ballal et al. [79] presented electron diffraction evidence from a cross-sectioned cBN film showing strong peaks in the cBN {111} and {220} rings indicating a strong preferential orientation that they interpreted as a [110] out-of-plane texture. Medlin et al. [206] have presented similar data, but show that the data can be also interpreted as a [111] *in-plane* (or 'double-fiber') texture. This preferential orientation is analogous to the [0002] in-plane texture observed in the graphitic BN layer. Specifically,

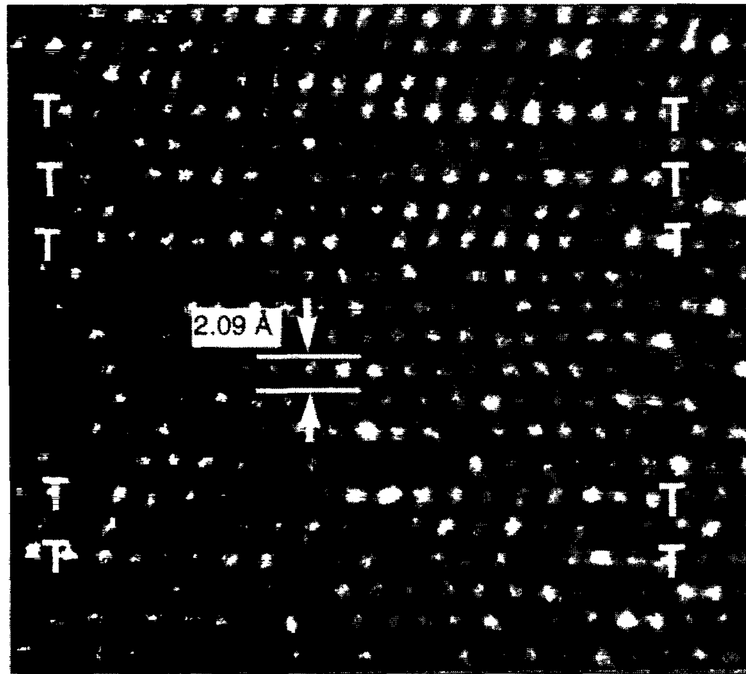

Fig. 14. HRTEM image of a twinned cBN crystallite. {111} fringes are horizontal on the image and the twins and stacking faults are designated by T. From Medlin et al. [80].

the cBN is preferentially oriented such that individual crystallites have at least one [111] direction lying in the plane of the film but are otherwise randomly oriented about (i) the substrate normal and (ii) the in-plane cBN [111] axis (see Fig. 13(d) and Fig. 15). [9] A review of diffraction patterns published in the literature suggests that a [111] in-plane texture is common in cBN films grown on a variety of substrates [132,139,146].

Several explanations for the preferential cBN orientations have been proposed. Ballal et al. [79] suggested a surface-energy argument, suggesting that a [110] out-of-plane orientation might arise if cBN prefers to grow on a non-polar face since the (110) planes have an equal density of boron and nitrogen atoms. Using the same type of analysis described above for hBN, McKenzie et al. [207] showed that the Gibbs energy of elastically strained cBN is lower if a [111] direction is within rather than perpendicular to a plane of biaxial stress. Therefore, they proposed that the [111] in-plane texture of cBN results because it is the most thermodynamically favorable texture. Johansson et al. [160] also advocate this proposal. However, after extending the elastic-strain analysis to include all relative orientations of stress/strain fields to the crystal directions, Cardinale et al. [200] showed that while the [111] in-plane texture possesses a lower Gibbs free energy than the [111] out-of-plane texture, it is not the global minimum.

However, it may be significant that the crystallographic orientations in the cBN layer are such that the cBN {111} planes form parallel to the tBN (0002) planes in the initial graphitic layer [206,208]. Alignment between the cBN {111} planes and the graphitic boron nitride basal planes might be anticipated due to the structural similarities of the two types of planes. Both consist of six-fold rings of alternating boron and nitrogen atoms with similar projected atomic dimensions. Several

[9] A [110] out-of-plane texture would be a special case of the [111] in-plane texture with the added constraint that two, rather that one, [111] directions must lie in the plane of the film.

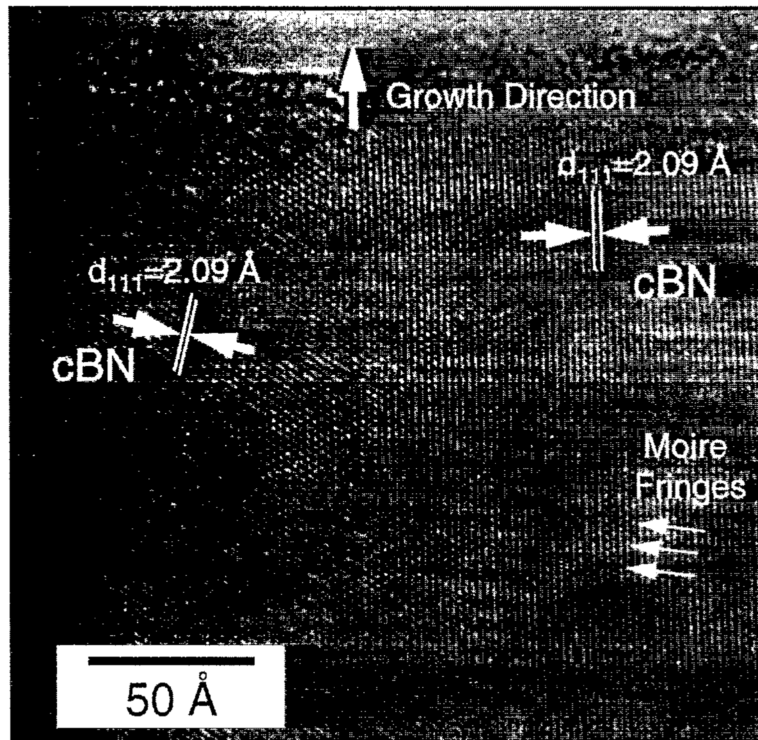

Fig. 15. HRTEM image taken near the top of a 250 Å thick cBN layer. The lattice-fringe spacing of 2.09 Å comes from the cBN {111} planes, one set of which is parallel to the marked growth direction (i.e. perpendicular to the substrate). From Mirkarimi et al. [137].

HRTEM studies have shown cases of local alignment between the tBN (0002) and cBN {111} planes [160,205,206,209], although the structural details at the sp^3/sp^2 interface remain unclear.

As discussed more thoroughly in Section 7, ion-induced compressive stress and densification have been proposed to play an important role in cBN synthesis. Thus, the preferential crystallographic alignments may reflect details of the growth mechanism. In 1995, Bewilogua et al. [208] suggested that the alignment results from the compression of hBN basal planes in the [0002] direction to form the cBN (111) planes. In 1994, though, Medlin et al. [80,83] considered such a transformation in the thin film case and pointed out that, as in the bulk transformation [30,34], direct compression of hBN produces the wurtzitic (wBN) phase rather than cBN. This is a result of the identical A A ′ A... stacking sequence of the hBN (0002) and wBN (0002) planes. If, indeed, the aligned cBN results from a direct *c*-axis compression of the graphitic basal planes, then the graphitic material would instead need to be arranged in the rhombohedral (A B C...) stacking arrangement. Direct compression of rBN leads directly to the A B C... stacking sequence of the cBN {111} planes [34,35,210]. The presence of rBN in boron nitride films grown by ion-assisted deposition has been observed [83]; however, its predominance remains unclear.

An alternative relationship may be that the oriented graphitic material serves as a preferential nucleation site for growth of the cubic phase rather than as a direct precursor [206]. In such a case, hBN rather than rBN could play a role. The relative spacings of the hexagonal boron nitride (hBN) (0002) (3.33 Å) and cBN {111} (2.09 Å) planes approach a 3:2 ratio such that every third cBN (111) plane (stacked in a three-layer ABC... sequence) could be closely matched (within 6%) with every alternate hBN (0002) plane (stacked in a two-layer A A ′... sequence) forming a semi-coherent interface:

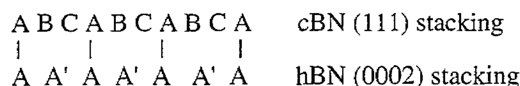

As drawn above, the planes labeled 'A' would maintain continuity across the interface. Furthermore, the lattice mismatch would be eliminated by compression of the graphitic BN to 3.1 Å [101], which is conceivable under the large compressive stresses typical in cBN films. Such an orientation relationship would be similar to recent observations [211–213] and calculations [214] of CVD diamond nucleating on the prismatic planes (i.e. the edges of the (0001) sheets) in graphite for which $(0002)_{graphite} \| (111)_{diamond}$ and $2\bar{1}\bar{1}0_{graphite} \| \bar{1}10_{diamond}$. More recently, Widany et al. [215] have calculated that the analogous hBN/cBN interface should be strong, relatively unstrained, and stable. Resolution of these two pictures (either nucleation *from* or *on* the graphitic interlayer) awaits a detailed assessment of the structural configuration of the graphitic material adjacent to the cBN (configured as hBN, rBN, or some disordered average?) as well as that of the cBN/graphitic BN interface (continuous or discontinuous?). In either case, the structure of the graphitic material appears to play an important role in controlling the cBN formation.

6.4. Near-surface layer

Several groups have analyzed cBN films using the surface-sensitive techniques of EELS [101,109,120], Auger [55], and photoelectron (XPS) spectroscopies [216], and concluded that the near-surface regions are sp^2 bonded. Friedmann et al. [55] showed that the boron KVV Auger lineshape, which at 170 eV is sensitive to about the upper 10 Å, was that of sp^2-bonded BN, not cBN. Sené et al. [120] used EELS to estimate that at least the topmost two monolayers were bulk-like sp^2 BN. Park et al. [216] used XPS to estimate that the outermost 12 Å were sp^2-bonded BN, similar to the value of 10–20 Å measured by Hofsäss et al. using EELS [101]. These findings are not consistent with the surface reconstruction suggested by Reinke et al. [113] In the surface reconstructions of diamond and silicon, the top atomic layer substantially relaxes from an sp^3 environment and acquires some π-bonding character but much smaller relaxations occur in the adjacent few layers [217]. The reconstructed surface never physically or electronically becomes true graphite or its silicon analog. Instead of a true reconstruction, the evidence suggests that the cBN films are coated with a distinct layer of sp^2-bonded BN. That this near-surface region is sp^2-bonded BN means that material exists as graphitic BN before it is transformed to cBN below the surface.

We conclude this section by commenting that the layered BN microstructure has not been universally reported. We note that some early HRTEM observations suggesting strongly oriented cBN at the substrate interface [79,104] resulted from the misidentification of the tBN (0002) lattice fringes as cBN lattice fringes [80]. In addition, *heteroepitaxial* cBN growth on both Si(001) and diamond has been reported. The Si work used conventional or modified PLD [182,183,185,186,218], while the diamond work used PLD assisted by ~ 500 eV ions [192]. Such growth would be a technological breakthrough, opening the doors to the development of cBN-based active electronics. Since diamond is well established to grow epitaxially on certain faces of cBN single crystals [219], the development of diamond-based electronics would also be enabled. As discussed in Section 5.6, synthesis of polycrystalline cBN, yet alone heteroepitaxy, by conventional PLD has been unreproducible despite the extensive efforts of several groups. Furthermore, the phase characterization of one of the epitaxial cBN reports has been criticized [220]. The evidence of *heteroepitaxy* on diamond substrates was based on characterization by electron diffraction [192]. This result is in marked contrast to Kester et al. [133] who found no evidence in cross-sectional TEM for epitaxy or preferred orientation in cBN films deposited on diamond. At this time, given the limited characterization, absence of definitive

structural evidence, and lack of independent confirmation, it cannot be concluded that epitaxial cBN has been achieved.

- cBN films have a distinctive layered structure. From the substrate outward are: a thin amorphous layer, an sp^2-bonded layer, and finally the sp^3-bonded cBN.
- The basal planes of the sp^2-bonded interlayer are perpendicular to the substrate, i.e. the interlayer is textured with an in-plane [0002] orientation.
- The cBN is polycrystalline and consists of small, highly defective grains. Columnar grains whose height increases with film thickness are frequently observed.
- The cBN crystallites have one set of (111) planes perpendicular to the substrate (and parallel to the basal planes of the sp^2-bonded interlayer) but are otherwise randomly oriented. That is, the cBN layer is textured with an in-plane ⟨111⟩ orientation.
- The near-surface region of cBN films is sp^2 bonded.

7. Mechanistic issues in cubic BN film formation

Ion bombardment during film growth is critical in forming cBN films. In Section 4.1 we identified the important ion-bombardment parameters without discussing how ions might cause cBN formation. We now present and analyze several models that attempt to bridge this gap. Historically, many of these models have their foundations in models describing ion-induced formation of sp^3-bonded amorphous carbon. Simplified schematic representations of four proposed models are shown in Fig. 16.

7.1. Sputter model

Reinke and coworkers [111–113] have proposed a 'sputter' model in which cBN grows by the preferential sputtering of cBN relative to graphitic BN (see Fig. 16(a)). Indeed, significant amounts of sputtering can occur in cBN synthesis. For typical conditions, Reinke et al. show that over 60% of

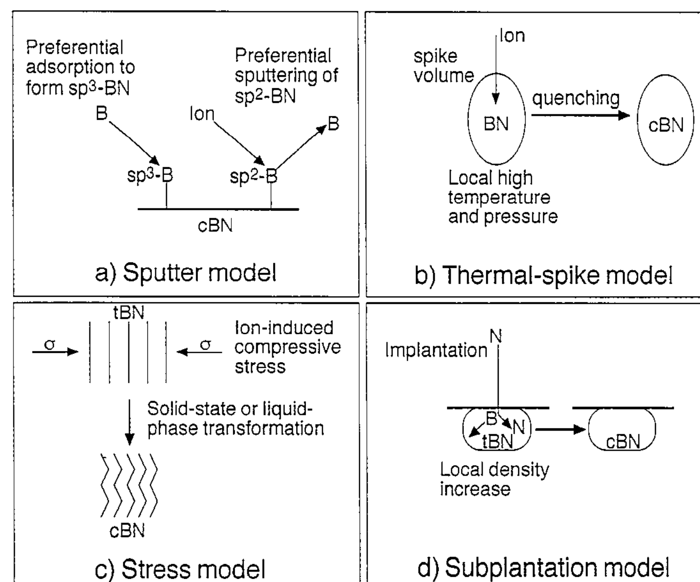

Fig. 16. Simplified schematic representations of (a) the sputter model, (b) the thermal-spike model, (c) the stress model, and (d) the subplantation model of cBN formation.

the incident boron atoms are sputtered [113]. They proposed that the tBN/cBN boundary (see Fig. 7) represents the transition to no tBN growth; that is, the ion flux at this transition is sufficiently high to etch all the deposited tBN. Only cBN growth then occurs because of its lower sputter yield. Two relationships form the primary support for the model. First, reasonable values of the sputter yields are obtained from the model using the experimental J/a values at the tBN/cBN and cBN/resputtering boundaries. Second, the J/a boundary, as estimated by Reinke et al., separating tBN from cBN formation and the inverse sputter yield of silicon have essentially the same energy dependence.

Hackenberger et al. [14] and Robertson [221] have previously discussed deficiencies about the sputter model. Some additional points follow, beginning with the two relationships mentioned above. We note that the experimental data used to formulate the model were obtained using constant conditions (e.g. ion flux and energy unchanging during growth). However, recent work [122,123] shows that fewer and/or lower energy ions are required to grow cBN once cBN nucleates (see Section 7.5). As recently discussed by Kulisch and Reinke [15], selective sputtering cannot be the phase-selecting process for these conditions. In addition, Hofsäss et al. [101] have recently grown cBN films under conditions (see Section 5.5) of very low sputter yield, which is inconsistent with the sputtering model. Concerning the agreement between inverse sputter yield and the boundary in J/a space separating tBN from cBN, the Si sputter yield presented in Fig. 3 of Reinke et al. [113] is nearly linear in energy. However, many related quantities, such as number of atomic displacements and vacancies generated per ion also have a linear dependence on energy (see, for example, the discussion of Mirkarimi et al. [108]). Therefore, a linear energy dependence alone cannot distinguish a sputter-dominated mechanism from mechanisms dominated by these other processes.

An additional concern about the model involves the nature of the surface because the sputter yield is inversely proportional to the surface binding energy [222]. It is known experimentally that the near-surface region of cBN films is sp^2 bonded (see Section 6.4). Thus the surface layer should sputter like sp^2-bonded BN, rather than sp^3-bonded BN, contrary to the needs of the sputter model. Finally, the model requires that newly deposited material be preferentially sp^3 bonded since preferential sputtering can only *purify* the phase content. Reinke et al. argue that cBN initially forms (nucleates) through a non-sputtering process but then grows by preferential sputtering. For the latter, sp^3 bonding can only result if an incoming atom preferentially sp^3 bonds on an existing sp^3-bonded surface site [113]. Under typical deposition conditions, the required preferential bonding at the surface is surprisingly high, nearly 100% [15]. It is difficult to reconcile the required high degree of preferential sp^3 bonding with the experimental fact that the surfaces are sp^2 bonded.

While preferential sputtering is not the mechanism of cBN growth by energetic processes, the sputter model has drawn deserved attention to the significant amount of sputtering that does occur.

7.2. *Quenching of thermal spikes*

Near the end of its trajectory in a solid, an ion will have insufficient energy to displace atoms. The ion energy will be dissipated into phonons in what has been termed a *thermal spike*. According to the analysis of Seitz and Koehler [223], these thermal spikes can result in very high temperatures (several thousand degrees Celsius) and pressures (up to 10 GPa) experienced locally over a very brief period of time (order of picoseconds). Early on, Weissmantel et al. suggested that thermal spikes could form cBN (see Fig. 16(b)). If the energy within the spike region is very rapidly quenched, they proposed that kinetics will favor formation of the metastable phase, cBN [224–226]. This mechanism is still proposed by some researchers. For example, Hofsäss et al. propose that cBN forms within the thermal spikes produced by subplantation [101]. In its current form the model is not quantitative enough to compare to cBN-growth experiments. However, rough estimates have indicated that the

spike diameters are several nanometers, much smaller than the cBN crystallite diameters of at least several tens of nanometers [108,113]. Thus cBN crystallites do not form from a single thermal spike (see also Section 7.5). Recently the understanding of ion/solid collisions has been improved using realistic atomistic simulations [227]. Such simulations show that melting does not occur within the thermal spike of high-melting-point ceramics such as hBN and cBN [228]. As noted in Sections 7.3 and 7.4, 'thermal spikes' have been incorporated directly into both the static stress model and the subplantation models. Usually in these models, however, the spikes are postulated to *hinder* cBN formation, either by relaxing stress or relaxing subsurface density increases through enhanced atomic mobility.

7.3. Stress-induced cBN formation

7.3.1. Static stress model

The ion bombardment that is critical to cBN synthesis also generates significant compressive stresses in the films [229,230]. In 1991, McKenzie et al. [11] suggested that cBN forms because the ion-induced stress places the BN material in the cBN-stable region of the thermodynamic phase diagram (see Fig. 16(c)). In a more detailed proposal [61,199,207], they coupled experimental data with a thermodynamic analysis. Above a particular value of the film stress (4–5 GPa), they observed that the cBN content increased dramatically, as shown in Fig. 17Mirkarimi. This threshold stress was found to be relatively insensitive to deposition conditions. Using the thermodynamic boundary between graphite and diamond estimated by Bermon and Simon [231], the equivalent boundary between hBN and cBN was estimated as ~ 3 GPa (see Fig. 17). That this estimated thermodynamic value (~ 3 GPa) was near the observed transition of cBN formation (4–5 GPa) was cited as support for the model.

Since McKenzie et al. [61] proposed their model, the BN phase diagram of Bundy–Wentorf has come under debate (see Section 2.2). Therefore, whether the thermodynamic boundary in the BN system will mimic that of carbon is uncertain. Furthermore, Cardinale et al. [229] and Reinke et al. [230] have shown that if cBN and hBN have the same ion-induced strain, cBN will have a much higher stress because of its higher elastic modulus. That is, since the effective modulus of the film

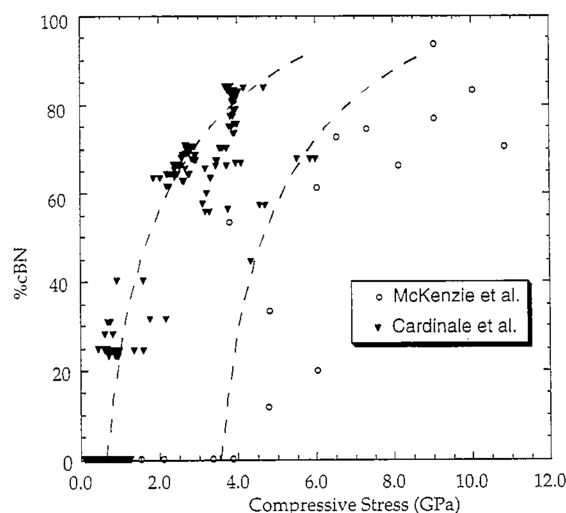

Fig. 17. Relationships between compressive film stress and cBN content observed by McKenzie et al. [61] and Cardinale et al. [229]. McKenzie et al. suggested that a critical stress was necessary to make cBN through a thermodynamic-like process. Adapted from Cardinale et al. [229].

increases with increasing cBN content, the stress will necessarily increase. While such an explanation does not predict the sharp stress transition observed by McKenzie et al., Cardinale et al. [229] did not observe a pronounced stress threshold in their measurements of residual stress versus cBN content (see Fig. 17).

McKenzie et al. [61] observed that the stress quickly rises to a very large value during the initial growth of cBN and then falls off with increasing deposition time. They suggested that the stress builds up until it drives the transformation to cBN. A similar stress evolution was observed in carbon films, and Puchert et al. [232] attributed the quick initial rise to a transition from discontinuous nuclei to a continuous film. Puchert et al. [232] suggested that this might also explain the dramatic changes in film stress observed in the initial stages of cBN film growth.

In the stress model, the substrate must be strong enough to support the film stress necessary to transform tBN to cBN [61]. Mirkarimi et al. [56] found a correlation between substrate hardness and cBN content (see Section 4.4). While these results are qualitatively consistent with the stress model, factors other than substrate strength cannot be ruled out for the difficulty in forming cBN on soft substrates.

As discussed in Section 4.1, cBN synthesis is very sensitive to ion-bombardment parameters such as the ion momentum. Assuming that stress is important to cBN synthesis, then how is stress related to these irradiation conditions? Is there any link between ion momentum and stress, and once the stress is generated, how does the tBN transform to cBN? These questions will now be discussed.

Ion bombardment is well known to cause increased compressive stress through densification and void removal in a process dubbed 'ion peening' [233]. Reviewing the literature, Windischmann [234,235] found that the compressive stress in ion-assisted film deposition tends to scale as the ion momentum (Eq. (4)). Since the threshold for cBN formation also scales as the ion momentum, at least for energies above several hundred electronvolts (see Section 4.1), there may be a correlation between compressive stress and cBN formation. However, there are exceptions to stress/ion-momentum scaling, and it has not been determined if *stress* scales as ion momentum *for cBN*, particularly over the energy range of $\sim$300–1200 eV.

Windischmann [236] derived an analytic relation for stress in terms of the irradiation parameters:

$$\sigma = C\delta J E^{1/2} \quad (5)$$

where E is the ion energy, J is the ion flux, C is a constant, and δ depends upon the relative masses and atomic numbers of the ions and film atoms. Eq. (5) gives the frequently observed $E^{1/2}$ dependence of stress. Windischmann [236] assumed that the strain is proportional to the fraction of atoms displaced from their equilibrium sites in the collision cascade of the ion and that defects are frozen in (i.e. they do not anneal). However, Mirkarimi et al. [108] argued that Windischmann's use of Sigmund's [237] sputtering theory to calculate the fraction of displaced atoms is not consistent with the model description (i.e. strain $\propto$ number of displacements). Instead, they showed that in a frozen-defect model such as Windischmann's, strain and stress should scale as E^1. At the energies ($\sim$500 eV) and J/a ratios (about 1) typically used for cBN deposition, TRIM [125,126] simulations for BN indicate that each film atom is displaced away from its binding site in the order of 10 times (assuming the knock-on displacement energy is 10–30 eV) [108]. Despite this extremely large amount of damage, the material is not amorphous like carbon, but is crystalline cBN or poorly crystalline tBN. Thus the great majority of defects (vacancies and interstitials) anneal and are incorporated into the crystalline material. A static model with frozen defects, such as that of Windischmann, is therefore not well suited for incorporation in stress models of cBN formation.

Davis [238] used a Sigmund/Windischmann-type approach, but made the advance of incorporating film-deposition rates and relaxation of film stress and derived the stress relationship:

$$\sigma\alpha\frac{C_{o}E^{1/2}}{[(a/J)+kE^{5/3}]} \quad (6)$$

By incorporating relaxation processes, which are taken in the model to be solely due to ion-induced thermal spikes (see Section 7.2), the equation can account for the energy dependencies other than $E^{1/2}$ observed in the literature. The model is limited by its reliance on a Sigmund/Windischmann-type relation for defect production, the lack of distinction between vacancies and interstitials (an issue for crystalline materials), and the fact that defect-relaxation processes only occur by thermal spikes (via the Seitz–Koehler relation). McKenzie et al. [61] suggested that since the Davis stress relationship provides a reasonable fit to data of sp^3-bonded amorphous carbon formation, it is also applicable to their model of stress-induced cBN formation. For the cBN-forming conditions of $J/a \approx 1$, Eq. (6) reduces to approximately $\sigma \propto E^{-7/6}$. In the context of a stress-model for cBN formation, stress should rise with increasing ion energy for fixed J/a, since increasing ion energy also causes increased cBN content. Instead, Eq. (6) predicts that stress decreases as energy increases.

7.3.2. Dynamic stress model

Mirkarimi et al. [108] constructed a *kinetic* model of stress generation from ion bombardment. They note that strain, and as a consequence stress, is controlled by two factors: (i) the dynamic concentration of interstitials and vacancies, which gives an 'instantaneous stress', and (ii) the time-integrated accumulation (trapping) of defects at sinks, which controls the residual stress. The hydrostatic stress σ is proportional to the volumetric strain, ΔV, as:

$$\sigma \propto \frac{\Delta V}{V}=\frac{\Delta V_{\mathrm{i}}^{\mathrm{rel}}}{\Omega}C_{\mathrm{i}}+\frac{\Delta V_{\mathrm{v}}^{\mathrm{rel}}}{\Omega}C_{\mathrm{v}} \quad (7)$$

where $\Delta V_{\mathrm{i}}^{\mathrm{rel}}$ and $\Delta V_{\mathrm{v}}^{\mathrm{rel}}$ are the relaxation volumes associated with interstitials and vacancies, respectively, and Ω is the atomic volume. Although vacancy and interstitial concentrations are roughly equal, the absolute magnitude of the interstitial relaxation volume is greater than that of the vacancy relaxation volume and thus $\Delta V/V \neq 0$ (i.e. the instantaneous stress is non-zero). From a simplification of two coupled differential equations describing defect production and loss, Mirkarimi et al. [108] obtained a steady-state limit of the defect concentration (and by extension film stress) that was independent of deposition rate:

$$\sigma \propto C_{\mathrm{i}} \approx C_{\mathrm{v}}=C=\sqrt{\frac{J\dot{G}^{0}}{\alpha n}} \quad (8)$$

Here α is an experimental constant, J is the ion current density, n is the atomic number density, $\dot{G}^0$ is the spatially dependent production rate of ion-induced vacancies or interstitials. Eq. (8) implies that the maximum defect concentration (C_{max}), or maximum (critical) stress (σ_{max}), occurs when a film element is positioned to experience the maximum value of the defect production rate, $\dot{G}_{\mathrm{max}}{}^{0}$, and hence:

$$\sigma_{\mathrm{max}} \propto C_{\mathrm{max}} \propto \sqrt{J\dot{G}_{\mathrm{max}}{}^{0}} \quad (9)$$

Using $\dot{G}_{\mathrm{max}}{}^{0}$ values from TRIM simulations, Mirkarimi et al. [108] concluded that the maximum stress should scale approximately as ion momentum, i.e. $\sigma_{\mathrm{max}} \propto (mE)^{1/2}$. As noted above, a critical (maximum) stress is needed over some volume to induce the phase transformation in a stress model. Thus the model provides some physical justification for the $(mE)^{1/2}$ scaling observed in cBN synthesis, either within a model of stress-induced cBN formation, or within any model in which a critical (instantaneous) defect concentration is important.

The model can account for energy dependencies other than $E^{1/2}$ by including the non-instantaneous (residual) stress that results from defect trapping at sinks. However, expansion of the model is limited by the lack of input parameters (rate constants, etc.).

The observation that cBN content falls off sharply below a critical deposition temperature is not currently described or predicted by the stress-type models. We note that the critical temperature for cBN synthesis ($\gtrsim 100$ °C) is close to the temperature for interstitial diffusion in diamond (~ 200 °C) [239], and perhaps a more refined defect model can account for the temperature dependence of cBN formation. Also, if a certain sp^2-bonded precursor is necessary besides stress to nucleate or grow cBN [83], the temperature dependence of the precursor may play a role.

Different interpretations are possible within the models of stress-induced cBN formation. Compressive stress could convert sp^2-bonded BN to cBN via *macroscopic* compression in bulk-like manner. Alternatively, the instantaneous stresses over a *microscopic* area (several to tens of angströms) could locally transform sp^2-bonded BN to cBN in an incremental manner during film growth. As discussed in the next section, this second possibility is qualitatively similar to 'subplantation' with some subtle distinctions. In both the static and dynamic versions of the stress model, sufficient stress is necessary to drive the transformation to cBN. However, a large residual stress must not necessarily remain afterwards.

7.4. Subplantation

Lifshitz et al. [240,241] coined the term 'subplantation' to describe their model for the formation of sp^3-bonded carbon by ion irradiation. They proposed that if ions of sufficient energy penetrate below the surface of sp^2-bonded carbon, the ions will displace more sp^2-bonded atoms than sp^3-bonded atoms, resulting in an accumulation of sp^3-bonded sites. Their proposal relied on older studies indicating a significant difference in the displacement energies (E_d) of sp^2-bonded carbon ($E_d \approx 35$ eV) and sp^3-bonded carbon ($E_d \approx 80$ eV), i.e. $\Delta E_d \approx 45$ eV. Robertson [239,242] notes that more recent measurements indicate a much smaller difference in the displacement energies ($\Delta E_d \leq 10$ eV), and a simulation of this mechanism at higher energies disagreed with experimental observations.

The model of Davis [238] (see Section 7.3) was used to explain the energy dependence of sp^3-bonded carbon formation from ion-induced compressive stress. Using the terminology of a subplantation-like mechanism, Robertson [239] independently derived a similar relation. In this version of subplantation, sufficiently energetic ions penetrate the surface and enter interstitial positions, temporarily increasing the local density. Robertson proposed that the local bonding 'adjusts' to an sp^3 hybridization in response to this local density increase (see Fig. 16(d)). On a conceptual level this mechanism is similar to the stress mechanisms with the following distinction: The dynamic stress model asserts that the increased density and volumetric strain generates stress that converts sp^2- to sp^3-bonded carbon (i.e. the density increase *indirectly* results in sp^3-bonded carbon). The subplantation model asserts that the density increase *directly* results in sp^3-bonded carbon. Both perspectives have to account for the density increase accompanying increased sp^3-bonding. Within the subplantation model, density increases primarily because of a local mass increase. Within the dynamic stress model, density increases primarily because of a local volumetric decrease. A more general perspective, which encompasses both of these interpretations, is that the ion irradiation raises the free energy of the sp^2-bonded material until it is higher than the metastable sp^3-bonded carbon. Assuming a small kinetic barrier, the material then transforms. This approach is discussed in general for ion-induced phase transformations by Nastasi and Mayer [243] and has been discussed in the context of cBN formation by Friedmann et al. [55]. While sp^3-bonded carbon is metastable, the analogy will not hold if the

thermodynamically stable phase at ambient is cBN (see Section 2.2). Furthermore, such free-energy arguments do not provide insight into the microscopic mechanism of the transformation.

As noted in Section 7.3, the Davis stress model [238] (Eq. (6)) does not predict the observed energy and ion-flux dependence for cBN formation. Specifically, stress is predicted to decrease with increasing energy at energies of several hundred electronvolts and ion-to-atom ratios close to one. Similarly, Robertson's subplantation model [239.242], which has effectively the same energy and ion-flux dependence, also fails to describe cBN formation. That the models which might work for describing sp^3-bonded carbon film synthesis, do not necessarily work for cBN film synthesis is not surprising. For example, as noted by Dworschak et al. [50], Hofsäss et al. [132], and Robertson [221], because BN has a much higher ionicity than carbon, BN does not amorphize nearly as readily (if at all). Additionally, carbon films are typically deposited at low (≤ 150 eV) ion energies, and the sp^3 fraction decreases with higher ion energies. In contrast, sp^3-bonded BN (cBN) can be deposited with ion energies of over 1000 eV. Finally, carbon films with high sp^3 content cannot be deposited at temperatures greater than several hundred degrees Celsius [244]. In contrast, cBN films can be deposited at temperatures up to at least 1300 °C [121].

Dworschak et al. [50] have proposed another argument for a subplantation-type model. They used TRIM simulations to estimate the local difference between the number of interstitials and vacancies per unit depth (i.e. a local density change). The spatial offset in vacancy and interstitial concentrations occurs because an interstitial is on average knocked forward from the point of vacancy/interstitial production. For 500 eV ions, the density increase below the surface became larger as ion mass is increased. Thus the model predicts an increase in cBN content with increasing ion mass, consistent with experimental observations for constant ion flux. For a given flux of argon ions, their analysis predicts an increase in cBN content from 200–300 eV and a decrease in cBN content from 300–1200 eV. Unfortunately, comparison to experiment is complicated by the presence of the resputtering boundary (see Fig. 7). Their model is in good agreement with the energy dependence of sp^3-bonded carbon.

Recently, Robertson [221] modified the subplantation model to better describe cBN formation. As do Mirkarimi et al. [108], Robertson takes a kinetic approach and considers production and recombination of both vacancies and interstitials. Robertson assumes that interstitials condense to form extended defects, in addition to combining with vacancies, and that these extended defects result in cBN formation. The cBN formation rate was assumed to be proportional to the interstitial concentration squared. This choice, when combined with the loss rate of cBN sites because of thermal spikes, allows elimination of the defect concentration from the relationships. Although Robertson approximates that the vacancy and interstitial concentrations are the same, the rate equations include no terms accounting for the extra vacancies left over when the interstitials are used in cBN production. The net formation rate of cBN sites (i.e. the cBN fraction), n, is then:

$$n=\frac{k_1 E_{1/2}}{\frac{1}{\phi}+0.016\ \frac{p}{E_0^{5/3}}\ E^{5/3}}$$

where k_1, p, and E_0 are approximate constants, ϕ is the ion flux, and E is the ion energy. The energy dependence is similar to that of the previous subplantation-type model for carbon, and hence does not describe cBN formation very well.

As described in Section 4.1, there is a sharp increase in cBN content above some critical ion-to-atom value. As discussed by Reinke et al. [113], the current subplantation models do not account for such a sharp transition. Analogous to the critical stress proposals, however, a critical density may be

necessary to drive the transformation. Also, as with the other models, the subplantation models do not currently account for the sharp temperature threshold below which cBN does not form.

7.5. Nucleation versus growth

As discussed in Sections 4.1 and 4.3, once a cBN layer has nucleated, cBN growth can proceed using lower energy ions or lower substrate temperatures. Differences in nucleation and growth also have implications for the cBN microstructure. Robertson noted that in a nucleation and growth model, the crystal size is related to the separation of nuclei, not to the diameter of thermal spikes [221]. Since nucleation is more difficult than subsequent growth, the cBN-formation boundaries in plots such as Fig. 7 are actually the boundaries for cBN nucleation. The extremely strong dependence of nucleation processes to parameters such as temperature and strain may account for the sharpness of the cBN-formation boundaries. Whether the boundaries for cBN *growth* are as sharp as those for nucleation has yet to be determined. Additionally, it is not yet known whether the nucleation mechanism is distinct from the growth mechanism, or whether the mechanisms are basically the same but have different energetic requirements. Being able to use less rigorous conditions for growth offers exciting possibilities to increase the rate of deposition and improve the crystalline quality.

7.6. Mechanism summary

Clearly none of the simple models described above gives a completely satisfying picture of cBN formation. Instead, each model tends to focus on a single aspect of a complicated process that involves significant ion damage, densification, and phase transformation. We close this section by highlighting a few key points and unanswered questions about cBN synthesis that must ultimately be answered by a comprehensive model.

That the widely observed layer of sp^2-bonded BN between the substrate and the cBN layer is oriented is almost certainly because of the ion-induced compressive stress [61]. The pathway may include plastic deformation [200,201]. Whatever the role of stress in cBN nucleation, it has been suggested that once the basal planes of the sp^2-bonded interlayer are perpendicular to the substrate, the inability to further plastically deform allows the stress level to rise substantially [201]. For typical ion-assisted processes, cBN nucleation is sufficiently difficult as to occur only marginally before total resputtering of the film occurs [113]. cBN nucleation requires a higher temperature and more ion energy than subsequent growth (see Section 7.5). Whether this is true because the growth and nucleation mechanisms are different is not known. However, it is not clear why different mechanisms are necessary.

For at least some deposition conditions, columnar grains extend from the bottom to the top of the cBN layer (see Section 6.3). Thus significant grain growth can occur and the grains are significantly longer than the ion-penetration depth. The cBN films are capped by a distinct layer of sp^2-bonded BN (Section 6.4). As the film thickens, this graphitic layer is in turn coated over and must be transformed to the much denser cBN phase at some point below the surface [55,101,108,245]. The local structure of the graphitic BN may be important to the transformation mechanism. As discussed in Section 6.3, this may be related to the in-plane [111] texture that is observed in the cBN layer. Understanding the microscopic details of how this transformation occurs and results in grain growth is important and will require much experimental and computational effort (see Fig. 18).

Regardless of the transformation mechanism, below the surface, the density of the graphitic BN material increases because of ion implantation. This, combined with strain resulting from ion-generated defects, produces substantial compressive stress. Ion irradiation of the polycrystalline cBN produces

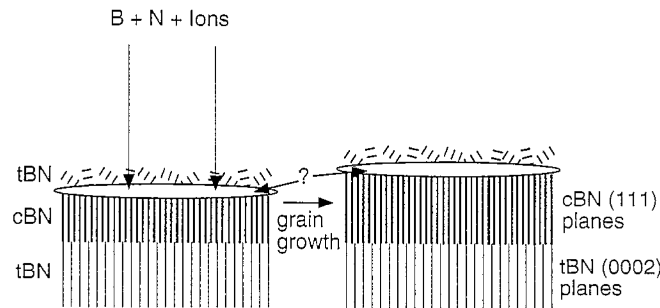

Fig. 18. Schematic illustration of growth of a cBN crystallite. The heavy lines represent (111) planes of cBN while the light lines represent basal planes of tBN. Whether the surface tBN layer is preferentially oriented is not known. Under the influence of ion irradiation, the cBN (111) planes lengthen when the near-surface tBN is overgrown and transformed to cBN. The structure at the upper cBN/tBN interface and the transformation pathway are not known, as labeled by the question mark.

strain-generating defects, which in turn produce significant residual compressive stress because of the extremely high elastic modulus of the cBN [229,230]. This residual stress, combined with environmental factors, leads to poor film adhesion (see Section 9.1).

- The texture of the graphitic BN interlayer appears to result from ion-induced compressive stress.
- cBN formation occurs below the film surface, where sp^2-bonded BN is transformed to cBN.
- Both density-driven and stress-driven models of the transformation have been proposed and widely discussed.
- The microscopic pathway of the tBN to cBN phase transformation is not known.

8. Mechanical and electronic properties of cBN films

8.1. Mechanical properties

8.1.1. Bulk cBN

Before discussing work on the plastic and elastic properties of cBN thin films, we briefly review the mechanical properties of bulk cBN. Generally, hardness is measured through microhardness or nanoindentation testing [246,247]. In Vickers or Knoop microhardness measurements, the size of the indent made at a known load is usually measured optically. In nanoindentation, hardness is typically measured using a three-sided Berkovitch indenter without having to image the indent. The tip shape of the Vickers and Berkovitch indenters are quite similar, but both are dissimilar from the shape of a Knoop indenter. Microhardness values are typically given in kg mm^{-2}, whereas nanoindentation hardness values are typically given in GPa. The kg mm^{-2} values can be multiplied by 0.0098 to yield GPa values. This is almost a factor of 100, i.e. 5000 kg $mm^{-2} \approx 50$ GPa. As shown in Table 6, cBN (Vickers hardness of roughly 50 GPa) is the hardest material after diamond (Vickers hardness of 80+ GPa).

Unfortunately, single crystals of cBN only up to about 0.5 mm in diameter are available. Grimsditch et al. [255] performed Brillouin scattering measurements on individual cBN grains and obtained C_{ij} elastic modulli (see Table 6) in good agreement with recent theoretical work [257,258].

8.1.2. cBN films

Obtaining good estimates of cBN *film* hardness has been problematic. One reason is the difficulty, due to adhesion problems, in growing cBN films thicker than a few thousand angströms (see Section

Table 6
Mechanical properties of bulk cBN

Hardness, H	45–55 GPa	Vickers — polycrystalline	[2,5,248]
	≈55 GPa	Berkovitch/Nanoindentation—polycrystalline	[137]
	40–60 GPa	Knoop — polycrystalline	[30,249]
	30–93 GPa	Knoop — single crystal (depending upon orientation)	[250]
Young's modulus, E	800–900 GPa	Various Methods — polycrystalline	[137,229,251,252]
Bulk modulus, B	370–385 GPa	Pressure dependence of lattice parameter	[253,254]
	400 GPa	Brillouin Scattering— single crystal	[255]
C_{11}	820 GPa	Brillouin Scattering— single crystal	[255]
C_{12}	190 GPa	Brillouin Scattering— single crystal	[255]
C_{44}	480 GPa	Brillouin Scattering— single crystal	[255]
Fracture toughness, K	2.8 MPa $m^{-1/2}$	Single crystal	[256]
	3.5–5.0 MPa $m^{-1/2}$	Polycrystalline	[248,249]

9.1). For such thin films, indent depths of less than 50 nm are required to keep the depth within the recommended value of roughly 10–20% of the film thickness [246,259,260]. Such shallow indents can render spurious results even in nanoindentation. For indents beyond roughly 20% of the film thickness, substrate effects can become substantial. Applying the Hainsworth–Page method [261] to cBN films on Si, Mirkarimi et al. estimated that the substrate begins to elastically deform at an indent depth to film thickness ratio of about 0.12 [137]. Such a substrate effect will alter the elastic modulus determined by indentation more than the measured hardness. Another possible obstacle is the elasticity of composite or layered BN films. As discussed below, some researchers have reported hardness values near or above bulk values even though the substrate is much softer and substrate effects should be substantial. Microhardness measurements are particularly susceptible to the effects of elastic recovery; however, the indent diagonal lengths are believed to be only moderately affected by the recovery process [247,262]. While accounting for modest elastic effects, nanoindentation may overestimate the hardness of *highly* elastic materials.

Some early studies [103,104] estimated the hardness unconventionally by scratching the film surface with various materials of known microhardness. For example, Inagawa et al. [103] estimated a hardness of 4000 kg mm^{-2} for 1000–3000 Å thick cBN films.

Andoh et al. [263] reports a Knoop microhardness (H_K) of 4900 kg mm^{-2} using a 15 g load on a 3000 Å thick BN film on Si. The indent depth should be approximately 2300 Å under these conditions, or a substantial 77% of the film thickness. Using 10 g loads on BN films, Murakawa et al. [147] measured H_K of 42–61 GPa (i.e. roughly 4200–6100 kg mm^{-2}) for cBN, 25–28 GPa for irradiated hBN/tBN, and 16–18 GPa for the Si substrate. The film thicknesses were not reported but are believed to be no more than several thousand Å for the cBN films. Thus the indent depth would have been a substantial fraction of the film thickness. Mineta et al. [151] reports $H_K = 3800–4600$ kg mm^{-2} using a 25 g load on 1.5 μm thick BN films. However, no evidence was provided to show that these thick BN films were predominantly cBN. Similar hardness values were obtained on WC–Co, TiN-coated WC–Co, and Si_3N_4 substrates. Using 5 g loads, Nishiyama et al. [145] reported Knoop hardness values of up to 4300 kg mm^{-2} for 3000 Å thick films of unknown cBN content. In that work, the indent depth was 50% of the film thickness and the Knoop-indent diagonal was only 4 μm, which would be difficult to measure accurately in an optical microscope. They observed that the hardest films also had the poorest adhesion.

Lin et al. [135] reported a Vickers microhardness (H_V) on BN films of 4300 and 2700 kg mm^{-2} using 5 and 10 g loads, respectively. With the film thickness somewhere between 1000–2700 Å, and even for a 5 g load, the indent depth is greater than the film thickness. Also, the cBN content of the

films is ambiguous because an SiO_2 buffer layer was used. Inagawa et al. [193] report $H_V = 5500$–6300 kg mm^{-2} on cBN films that were 1.5 μm thick. A silicon nitride buffer layer was said to allow for this remarkably thick cBN film to be deposited. No evidence was provided to support the claim that the 1.5 μm thick layer was predominantly cBN. Wada and Yamashita [130] reported $H_V = 4500$–5500 kg mm^{-2} for a 10 g load on a ~4000 Å thick cBN film. Here, the indent depth of ~4000 Å is about equal to the film thickness and substantial substrate effects would be expected. Kulikovsky et al. [72] observed $H_V = 2300$ kg mm^{-2} on tBN films using a 5 g load, and found decreasing hardness with increasing deposition temperature and BN crystallinity. At temperatures exceeding 500 °C, the H_V fell below 1200 kg mm^{-2}, the measured hardness of Si (111).

McKenzie [199] performed nanoindentation hardness (H_N) measurements using a Berkovitch tip on cBN and irradiated tBN films. The reported H_N of cBN was 58 GPa, where the indent depth was 1100 Å. The film thickness in this study was in the range of 1000–1500 Å [264]. The loading/unloading curve shows that the material exhibits an extremely elastic behavior. The irradiated tBN had $H_N = 20$ GPa, where the indent depth was 1800 Å, and the loading/unloading behavior was less elastic than that observed for cBN. Dworschak et al. [68] reported $H_N \approx 40$ GPa on 1200 Å thick BN films that were predominantly cBN. While the loading/unloading curve was not shown and the indent depth was not stated, a reasonable depth would penetrate through most of the film thickness.

Lüthje et al. [139] report a nanoindentation hardness (H_N) of 60 GPa on cBN:C films with thicknesses ≤2500 Å. The films contain ~5% carbon from the processing conditions. No details of the hardness testing procedure were stated. Johansson et al. [265] performed nanoindentation measurements on films similar to those of Lüthje et al., and suggested that the high elasticity of the oriented tBN:C layer between the cBN:C film and Si substrate serves to increase the apparent hardness. The indent depth was 60 nm in both the 400 nm thick tBN:C and 200 nm thick cBN:C films, and the elastic recovery was 83%, 72%, and 73% for the tBN:C, cBN:C films, and Si substrate, respectively (where 100% = fully elastic). Since (i) several groups using different techniques have reported hardness values for cBN films near or exceeding bulk values, measured under conditions where the indent depth is 50–100% of the film thickness, and (ii) the Si substrates are >4 times softer than bulk cBN, and substrate effects are expected to be significant, it is likely that the 'apparent hardness' is enhanced in some manner.

Recently Mirkarimi et al. [137] deposited 7000 Å thick cBN films (see Section 9.1), and performed nanoindentation measurements using indent depths of 1000 Å. Using a conventional Oliver–Pharr [266] analysis of the loading/unloading curves, hardnesses of >60 GPa were measured. An example of the loading/unloading curve on a cBN film is shown in Fig. 19. The measured elastic modulus was lower than the expected value, and this was attributed to substrate effects. Analysis using

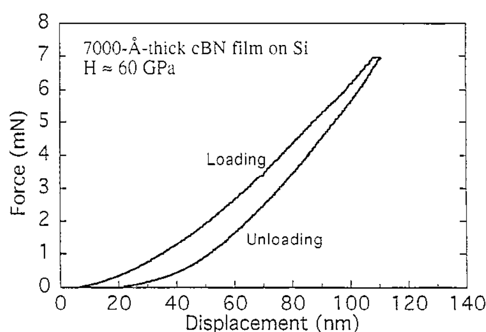

Fig. 19. Nanoindentation analysis of a 7000 Å thick cBN film on a silicon substrate. The left-most trace is the loading curve while the right-most trace is the unloading curve. Analysis of the unloading curves gives a hardness of ~60 GPa. From Mirkarimi et al. [137].

the Hainsworth–Page method [261] suggests that the substrate begins to affect the measurement of the elastic modulus at an indent depth to film thickness ratio of 0.12 (12%). Analysis of the loading/ unloading curves using finite-element modeling gave a high yield strength (about 50 GPa) and an elastic modulus close to the bulk value.

8.2. Electronic properties

In addition to hard-coating applications, cBN has potential for use in high-power, high-temperature electronic devices. cBN is a wide-bandgap semiconductor and, unlike diamond, it has been doped *both* n- and p-type (see Table 7). As thermal-budget issues become more important with increasing miniaturization in integrated circuits, the high thermal conductivity [1] (2–9 W cm^{-1} K^{-1}) of cBN makes the material well suited for electronic applications. For bulk cBN synthesis, the crystalline perfection has improved to the extent that a light emitting diode (LED) fabricated by Misima et al. [8,10,269] operated up to 630 °C and emitted primarily in the ultraviolet ($\lambda < 390$ nm) region. However, emission out to $\lambda \approx 600$ nm occurred and was believed to result from inhomogenities in structure and doping.

There are few reports of the electronic properties of cBN films, which is likely because of the difficulty in synthesizing nearly phase-pure and highly crystalline films. Ronning et al. [270] have reported a resistivity (ρ) of 10^{9}–10^{10} Ω cm for predominantly cBN films, which is close to the reported intrinsic value for bulk cBN. Recent work on GaN, a similar wide-bandgap material, has shown excellent performance as a light-emitting diode operating in the blue region of the spectrum [271]. This is despite a high dislocation density [271], contrary to standard III–V diode materials. However, current cBN film technology generates films that are greatly inferior to typical GaN films in crystalline quality. In addition, cBN has an indirect electronic bandgap [272], which is not ideal for light-emitting diodes.

Most of the reports on the electronic properties of cBN films have come from the Warsaw group [273–277] who have used films deposited by a pulsed-plasma deposition technique. Because the documentation [273,277,278] presented thus far makes it difficult to estimate the cBN content of the films, the results are not discussed further here. Phani et al. [279] reports unintentionally obtaining n-type conductivity in cBN films and speculated that this arose from carbon impurities introduced during the deposition process. Further characterizing the phase of these films is highly desirable (see Section 3), however. Lu et al. [150] measured the electrical properties of mixed-phase BN films with cBN percentages as high as 33%. For the two films with cBN percentages between 28–33% doped p-type using Mg, they observed resistivities of 0.07–0.10 Ω cm, carrier concentrations of $1–4 \times 10^{18}$ cm^{-3}, and mobilities of 22–47 cm^2 V^{-1} s^{-1}.

Gubanov et al. [280] conducted a theoretical study of the defect states in cBN, and observed that Si doping at B sites can account for the observed n-type conductivity. In a related work [281] they also suggest that, in the absence of doping, boron and nitrogen vacancies can be 'p-type' and 'n-type', respectively, when the composition deviates from ideal stoichiometry.

Table 7
Electrical properties of cBN

Bandgap (eV) [1,5]	p dopants [8,267]	n dopants [8]	$\rho_{intrinsic}$ (Ω cm) [1,5]	$\rho_{extrinsic}$ (Ω cm) [1,268]
≥6 eV (indirect)	Be, Mg	Si, S, KCN	10^{10} (@20 °C)	10^{2}–10^{3} (p) 10^{3}–10^{4} (n)

As feature sizes become smaller in microelectronic devices, there is a drive to reduce capacitance effects by replacing SiO_2 with insulating layers having lower dielectric constant, ϵ, where $\epsilon(SiO_2) \approx 4$. Cameron et al. [173] and Karim and Cameron [282] report that mixed-phase BN films (<30–40% cBN) deposited by plasma-assisted CVD yield $\epsilon \approx 2.2$–4.4, which is surprising since the bulk values for hBN and cBN are 5.9 and 7.1, respectively [283]. Sullivan et al. [284] measured the dielectric constants of BN films with $\geq 85\%$ cBN deposited by ion-assisted PLD and found $\epsilon \approx 6.5$–8.0, close to bulk cBN, while Ronning et al. [270] found the slightly higher values of $\epsilon \approx 8$–10 for their cBN films. tBN films deposited by ion-assisted PLD also had dielectric constants close to bulk values [284]. However, tBN films deposited by plasma-assisted CVD yielded ϵ values as low as 3.75 [284]. Sullivan et al. [284] suggested the PACVD films in the previous studies [173,282] had dielectric constants below bulk values because the density was below bulk values. Even given low dielectric constants, whether *porous* BN films would meet the many other requirements for an interlayer dielectric is questionable. In particular, hBN is known to be hygroscopic and susceptible to environmental degradation [285].

- Thick cBN films can be as hard as bulk cBN.
- The electronic properties of cBN films are not well investigated largely because of a lack of electronic-grade films.

9. Current barriers to application of cubic BN film technology

9.1. Adhesion

cBN films are widely observed to delaminate, particularly for thicknesses greater than a few thousand angströms. This undesirable attribute is thought to result from two factors: (i) compressive stress, and (ii) water in the ambient environment. The ion-bombardment conditions typically used to synthesize cBN generate high compressive stresses (see Section 7.3), and the substrate prevents the film from relaxing. The force on the substrate generally increases with increasing film thickness [286] and hence the maximum cBN film thickness will be limited by the adhesive strength. For instance, Inagawa et al. [193] observed that films >3000 Å thick delaminated after some period of time in air, whereas films >5000 Å thick delaminated spontaneously during deposition (in vacuum). Similar effects have been observed by many researchers at comparable or lower film thicknesses. For highly stressed films, Inagawa et al. [193] observed that delamination was less likely in vacuum or dry air than in atmosphere, so environmental factors are involved. In a systematic study, Cardinale et al. [197] placed highly stressed cBN films in either (i) vacuum, (ii) dry-oxygen, (iii) dry-nitrogen, or (iv) high-humidity environments. Films stored under high-humidity conditions delaminated within a day, while films stored in vacuum, dry oxygen, and dry nitrogen showed no signs of delamination after several weeks. The undelaminated films were subsequently placed under high-humidity conditions and delaminated within a day. Thus H_2O appears to have a much more deleterious effect on cBN adhesion than, for example, O_2. Cardinale et al. [197] suggested that water may react with BN according to the following reaction:

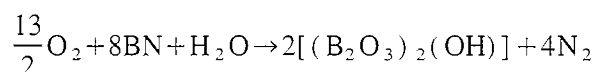

$$\frac{13}{2}O_2+8BN+H_2O\rightarrow 2[(B_2O_3)_2(OH)]+4N_2$$

The volumetric expansion at the interface accompanying reactions such as this would enhance film delamination. Hahn et al. [157] have subsequently measured an O/H ratio of 6.8 in their delaminated films, consistent with the O/H ratio of 7 expected from the above reaction.

Thus, the evidence suggests that stress and moisture are the primary factors contributing to cBN film delamination. However, all the above studies used silicon substrates, and whether these findings can be generalized to other substrates is not known. Since the film stress is largely intrinsic, rather than from thermal mismatch, it should not be a strong function of the substrate type, as long as the substrate can support the stress. The hydrolysis component of the delamination process may have a substrate dependence, i.e. matrix effects might influence the chemical reaction cited above. Also, the adhesive strength at which delamination occurs may change with the substrate and thereby change the maximum tolerable film stress. The literature indicates that there is no significant improvement in cBN film adhesion when non-silicon substrates are used [56,133,143], with the exception of better adhesion on diamond substrates [133,143].

Film adhesion has been improved by depositing buffer-layer films between the substrate and the cBN film and by using ion-mixing techniques. Okamoto et al. [140] observed that, although cBN films deposited directly on silicon delaminated readily in air, use of an intermediate boron layer and a graded BN_x layer beneath the cBN layer prevented film delamination for longer than six months air exposure. Inagawa et al. [193] tried graded buffer layers of the form $B_xN_yZ_{1-x-y}$ (where Z = C, Si, Ge, Al, Fe, Ti, and Cr) between the cBN film and silicon substrate. Only two of the buffer layers, $B_xN_yAl_{1-x-y}$ and $B_xN_ySi_{1-x-y}$, provided a significant improvement in adhesion, and the Si-based buffer layer gave the most improvement. While cBN films greater than 3000 Å thick were susceptible to delamination, Inagawa et al. [193] reported that adherent cBN films up to 1.5 μm could be deposited when the $B_xN_ySi_{1-x-y}$ interlayer was used. This would be a significant advance; however, no evidence was provided to show that the 1.5 μm thick layer was predominantly cBN. Ikeda et al. [104] improved the adhesion of BN films on WC–Co substrates by using an irradiated BN_x buffer layer. The irradiated tBN ('iBN') and cBN films had estimated compressive film stresses of ~1.6 and ~4.0 GPa, respectively. The lower stress in a composite cBN/iBN film was said to contribute to the enhanced adhesion. Murakawa et al. [143] modified this process by using an additional Ti interlayer, resulting in the structure cBN/BN_x/Ti/WC–Co (where WC–Co is the substrate). Like Okamoto et al., Kohzuki et al. [287] used a B/BN_x buffer layer on Si and observed that, although the adhesion was improved, much better adhesion resulted if the buffer layer was deposited on a Si substrate bombarded with 20 keV B and N ions. Post-deposition annealing at 800 °C for 21 h had no measurable effect on films employing the former process, but increased the peeling load of films using the latter process.

In addition to buffer layers, multilayer approaches have also improved adhesion. Ikeda et al. [146] used repeated sequences of cBN/BN_x/Ti layers (~1 μm thickness) to form a 3 μm thick multilayer on WC–Co substrates. The thickness of the cBN layers was not stated and the cBN content was difficult to estimate. Using a related approach, Mirkarimi [161] sandwiched three cBN layers between very thin (50–100 Å) B_4C layers giving a total thickness of 2000–3000 Å. These films were adherent whereas single-layer cBN films grown under identical conditions and to the same thickness spontaneously delaminated. IR spectroscopy showed that the multilayer had nearly the same cBN content as a comparable single-layer film, indicating that the improved adhesion did not coincide with a significant reduction in cBN content. Mirkarimi observed, however, that a thickness limit exists for this technique, i.e. delamination occurred for multilayer films that were ~75% thicker.

As noted in Section 7.2, even the stress model of cBN formation does not require that there be *residual* stress in the films. Stress is only necessary (either locally or macroscopically) to drive the transformation to cBN, but not to maintain the cBN once formed. This raises the question of whether the stress can be removed after or during deposition. Several researchers have attempted post-deposition annealing at temperatures of 800–900 °C for tens of hours, with only limited success [122,146,177,287]. Annealing away stress during film synthesis by operating at higher deposition temperatures, however, is very promising. Using a sputter process with low-energy ions (~100 eV)

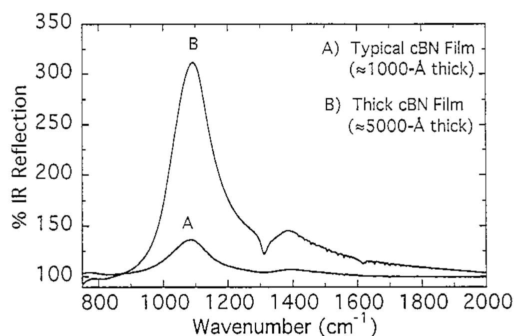

Fig. 20. FTIR reflection spectrum of a thick (~5000 Å) cBN film relative to a 1000–2000 Å thick cBN film. From Mirkarimi et al. [137].

and very low deposition rates (<0.1 Å s^{-1}), Kidner and Clarke [78] observed that films deposited at 950–1050 °C took greater than two months to delaminate whereas films deposited at temperatures ≤850 °C delaminated in less than one week. Taylor et al. [66,121] extended the process of Kidner and Clarke [78] by using higher deposition temperatures (1200 °C), longer deposition times (several tens of hours), and very low-energy (< 100 eV) nitrogen ions. They found that the frequency of the TO IR absorption decreased toward the bulk cBN value with increasing growth temperature, consistent with decreasing levels of compressive stress (see Section 3.1.4). Because of this, they [121] were able to synthesize thick (> 1 μm), adherent films with a high cBN fraction. Mirkarimi et al. [137] obtained cBN films up to 0.7 μm thick using a hybrid process based on three earlier techniques. The first and most important technique is that of Taylor and Clarke [121] and Kidner and Clarke [78] (high T, low E), the second technique is that of McKenzie et al. [122] and Hahn et al. [123] (higher ion energy for nucleation than subsequent growth), and the third technique is the use of B_4C sputter targets (similar to that used by Lüthje et al. [139] and Johansson et al. [117]). The FTIR spectrum of an ~5000 Å thick cBN film synthesized by Mirkarimi et al. [137] using this process is shown in Fig. 20 along with that of a 1000–2000 Å thick cBN film deposited at a lower substrate temperature. Thicker films enable the mechanical properties of cBN films to be accurately measured (see Section 8.1), as well as allow for a better understanding of the role of experimental parameters (temperature, ion energy, deposition rate, etc.) on film adhesion. However, even these newer processes need much improvement (most importantly, higher growth rates) for industrial viability.

9.2. sp^2-Bonded interfacial layer

As discussed in Section 6, regardless of the choice of substrate, an sp^2-bonded BN layer of several tens to hundreds of angströms thick usually forms before cBN nucleates and grows. In fact, there is no convincing evidence of uniform cBN film synthesis directly upon a substrate without an intervening sp^2-bonded interlayer. While Mirkarimi et al. [127] showed that the interlayer could be significantly reduced (to ≤10 Å) by depositing cBN on cubic SiC, this reduction was only observed along a small fraction of the film/substrate interface. For hard-coating applications, the sp^2-bonded BN interlayer *may be* an important problem. If the interlayer contributes significantly to the poor adhesion discussed above, or degrades mechanical properties, then it will need to be reduced or eliminated. However, this is not clear since some researchers have intentionally added a graded (irradiated) sp^2-bonded BN layer to improve film adhesion. The sp^2-bonded layer is a serious barrier to growth of epitaxial cBN films.

9.3. Commercializing ion-intensive deposition processes

Current routes to cBN synthesis require much higher ion-to-atom ratios than the energetic deposition processes used for other materials. Growth rates are limited by the available ion flux and are currently much lower than desired for industrial viability. Some improvement may be realized using the new knowledge that fewer or lower energy ions are required for cBN growth than for nucleation (see Section 7.5). Taking full advantage of this fact will demand very close process control and may require in-situ characterization of film phase, such as the in-situ ellipsometry technique demonstrated by McFall et al. [288]. Still, higher flux processes are clearly needed. Undoubtedly, the film-growth costs will be dominated by the cost of creating the ions, analogous to the costs of making the radical species (e.g. hydrogen atoms and methyl radicals) necessary for CVD diamond growth [289]. The narrow processing window for cBN formation will also make commercialization challenging since very uniform and matched fluxes will be required.

- The primary causes of cBN film delamination are residual film stress and water vapor.
- Post-deposition annealing has had limited success in removing film stress and promoting adhesion.
- High-temperature deposition has been successful in producing thicker (>0.5 μm) cBN films that are adherent.
- Buffer layers and multilayers can enhance film adhesion.
- The sp^2-bonded BN interlayer may limit some applications.
- Commercialization will require economical, high-growth-rate processes that give uniform, adhesive films over large areas.

10. Conclusions

Significant progress has been made in synthesizing nearly phase-pure cBN films by energetic deposition processes. In contrast to the situation for diamond film synthesis, there are no reproducible chemical or thermal routes to cBN-film synthesis. Compared to most energetic deposition processes, cBN synthesis requires much higher ion energies per film atom. The initial nucleation of cBN, in fact, occurs only over a rather narrow window of most process parameters, and this window is bounded by the condition where the film is totally sputtered (no net growth). Once nucleated, however, growth of cBN can occur under less energetic conditions.

Despite the many excellent studies conclusively synthesizing and correctly characterizing cBN films, we caution that many researchers still misidentify sp^2-bonded BN as cBN. Clearly the BN is sp^2-bonded as initially deposited and is transformed to sp^3-bonded BN under the influence of the energetic particle bombardment. There are plausible mechanisms explaining this transformation as either a stress-driven or density-driven process. However, the precise transformation route remains to be conclusively established.

The high compressive stress that is typically found in the highly defective cBN films leads to poor adhesion to the substrate. cBN does not nucleate directly on the substrate, but on top of or from an oriented layer of graphitic BN. Despite the presence of this softer interlayer, hard cBN coatings are being produced. Commercialization of the present energetic deposition processes will be challenging considering the cost of ion production, the required flux uniformity and tight process control necessary

given the narrow processing window, and the growth-rate limitations imposed by the need for copious amounts of ions.

Acknowledgements

This work was performed under USDOE contract DE-AC04-94AL85000 and supported in part by the Office of Basic Energy Sciences, Division of Materials Sciences. The authors thank G.F. Cardinale and T.A. Friedmann for comments on the manuscript. The authors also thank the many scientists in the cBN field with whom they have had interesting and valuable discussions.

References

[1] L. Vel, G. Demazeau, J. Etourneau, Mater. Sci. Engin. B 10 (1991) 149.
[2] H. Holleck, J. Vac. Sci. Technol. A 4 (1986) 2661.
[3] R.C. DeVries, in: R.E. Clausing (ed.), Diamond and Diamond-Like Films and Coatings, Plenum Press, New York, 1991, p. 151.
[4] R. Haubner, B. Lux, Diamond Relat. Mater. 2 (1993) 1277.
[5] R.C. DeVries, General Electric Company Corporate Research and Development Report No. 72CRD178, 1972.
[6] P.J. Gielisse, S.S. Mitra, J.N. Plendl, R.D. Griffis, L.C. Mansur, R. Marshall, E.A. Pascoe, Phys. Rev. 155 (1967) 1039.
[7] R.H. Wentorf, Jr., J. Chem. Phys. 36 (1962) 1990.
[8] O. Mishima, in: J.J. Pouch, S.A. Alterovitz (eds.), Synthesis and Properties of Boron Nitride, Materials Science Forum, Vol. 54/55, Trans Tech Publications, Brookfield, 1990, p. 313.
[9] W.A. Yarborough, J. Vac. Sci. Technol. A 9 (1991) 1145.
[10] O. Mishima, K. Era, J. Tanaka, S. Yamaoka, Appl. Phys. Lett. 53 (1988) 962.
[11] D.R. McKenzie, D.J.H. Cockayne, D.A. Muller, M. Murakawa, S. Miyake, S. Wantanabe, P. Fallon, J. Appl. Phys. 70 (1991) 3007.
[12] D.J. Kester, K.S. Ailey, R.F. Davis, K.L. More, J. Mater. Res. 8 (1993) 1213.
[13] S.P.S. Arya, A. D'Amico, Thin Solid Films 157 (1988) 267.
[14] L.B. Hackenberger, L.J. Pilione, R. Messier, in: F. Matacotta, G. Ottaviani (eds.), Science and Technology of Thin Films, World Scientific, Singapore, 1996.
[15] W. Kulisch, S. Reinke, Diamond Films Technol. 7 (1997) 105.
[16] F. Richter, in: Diamond Materials IV Electrochemical Society Proc., Vol. 94/95, eds. K.V. Ravi, K.E. Spear, J.L. Davidson, R.H. Hauge, J.P. Dismukes, The Electrochemical Society, Pennington, NJ, 1995.
[17] T. Yoshida, Diamond Relat. Mater. 5 (1996) 501.
[18] A.V. Kurdyumov, V.L. Solozhenko, W.B. Zelyavski, J. Appl. Cryst. 28 (1995) 540.
[19] R.S. Pease, Acta. Cryst. 5 (1952) 356.
[20] T. Ishii, T. Sato, Y. Sekikawa, M. Iwata, J. Cryst. Growth 52 (1981) 285.
[21] F.S. Galasso, Structure and Properties of Inorganic Solids, Pergamon Press, Oxford, 1970.
[22] R.R. Wills, Int. J. High Technology Ceramics 1 (1985) 139.
[23] R.H. Wentorf, Jr., J. Chem Phys. 26 (1957) 956.
[24] F.P. Bundy, R.H. Wentorf, J. Chem. Phys. 38 (1963) 1144.
[25] A. Herold, B. Marzluf, P. Perio, C.R. Acad. Sci. 246 (1958) 1866.
[26] B.T. Kelly, Physics of Graphite, Applied Science Publishers, London, 1981.
[27] J. Thomas Jr., N.E. Weston, T.E. O'Connor, J. Amer. Chem. Soc. 84 (1963) 4619.
[28] K.F. McCarty, P.B. Mirkarimi, D.L. Medlin, T.F. Friedmann, Diamond Relat. Mater. 5 (1996) 1519.
[29] G. Demazeau, Diamond Relat. Mater. 4 (1995) 284.
[30] F.R. Corrigan, F.P. Bundy, J. Chem. Phys. 63 (1975) 3812.
[31] V.L. Solozhenko, Thermochimica Acta 218 (1993) 221.
[32] S. Nakano, O. Fukunaga, Diamond Relat. Mater. 2 (1993) 1409.
[33] S. Bohr, R. Haubner, B. Lux, Diamond Relat. Mater. 4 (1995) 714.
[34] T. Sato, T. Ishii, N. Setaka, Commun. Am. Ceram. Soc. 65 (1982) C162.
[35] M. Ueno, K. Hasegawa, R. Oshima, A. Onodera, O. Shimomura, K. Takemura, H. Nakae, T. Matsuda, T. Hirai, Phys. Rev. B 45 (1992) 10226.
[36] D.R. McKenzie, W.G. Sainty, D. Green, in: J.J. Pouch, S.A. Alterovitz (eds.), Synthesis and Properties of Boron Nitride, Materials Science Forum, Vol. 54/55, Trans Tech Publications, Brookfield, 1990, p. 193.

[37] G. Turrell, Infrared and Raman Spectra of Crystals, Academic Press, London, 1972.
[38] M.H. Brodsky, in: M. Cardona, G. Güntherodt (eds.), Light Scattering in Solids I, Topics in Appl. Phys., Vol. 8, Springer, Berlin, 1982, p. 205.
[39] M.I. Eremets, M. Gauthier, A. Polian, J.C. Chervon, J.M. Besson, G.A. Dubitskii, Y.Y. Semenova, Phys. Rev. B 52 (1995) 8854.
[40] O. Brafman, G. Lengyel, S.S. Mitra, P.J. Gielisse, J.N. Plendl, L.C. Mansur, Solid State Commun. 6 (1968) 523.
[41] G.L. Doll, in: J.H. Edgar (ed.), Properties of Group III Nitrides, INSPEC, London, 1994, p. 245.
[42] R. Geick, C.H. Perry, G. Rupprecht, Phys. Rev. 146 (1966) 543.
[43] R.J. Nemanich, S.A. Solin, R.M. Martin, Phys. Rev. B 23 (1980) 6348.
[44] T. Sato, Proc. Japan Acad. 61B (1985) 459.
[45] J. Liu, Y.K. Vohra, T.J.T., S.S. Vagarali, Phys. Rev. B 51 (1995) 8591.
[46] G. Kessler, K.D. Bauer, W. Pompe, J.J. Scheibe, Thin Solid Films 147 (1987) L45.
[47] Light Scattering in Solids III, Topics Applied Physics, Vol. 51, eds. M. Cardona, G. Güntherodt, Springer, Berlin, 1982, p. 8.
[48] G.L. Doll, Sprong meeting of the Materials Research Society, San Francisco, CA, (1995).
[49] T.A. Friedmann, K.F. McCarty, E.J. Klaus, J.C. Barbour, W.M. Clift, H.A. Johnsen, D.L. Medlin, M.J. Mills, D.K. Ottesen, Thin Solid Films 237 (1993) 48.
[50] W. Dworschak, K. Jung, H. Ehrhardt, Thin Solid Films 254 (1995) 65.
[51] M. Kuhr, S. Reinke, W. Kulisch, Diamond Relat. Mater. 4 (1995) 375.
[52] P. Lin, C. Deshpandey, H.J. Doerr, R.F. Bunshah, K.L. Chopra, V. Vankar, Thin Solid Films 153 (1987) 487.
[53] D.M. Back, in: Physics of Thin Films, Vol. 15, Academic Press, Boston, MA, 1991, p. 287.
[54] Y.S. Yen, J.S. Wang, J. Phys. Chem. 93 (1989) 7208.
[55] T.A. Friedmann, P.B. Mirkarimi, D.L. Medlin, K.F. McCarty, E.J. Klaus, D. Boehme, H.A. Johnsen, M.J. Mills, D.K. Ottesen, J. Appl. Phys. 76 (1994) 3088.
[56] P.B. Mirkarimi, K.F. McCarty, G.F. Cardinale, D.L. Medlin, D.K. Ottesen, H.A. Johnsen, J. Vac. Sci. Technol. A 14 (1996) 251.
[57] S. Jäger, K. Bewilogua, C.-P. Klages, Thin Solid Films 245 (1994) 50.
[58] O. Tsuda, Y. Yamada, T. Fujii, T. Yoshida, J. Vac. Sci. Technol. 13 (1995) 2843.
[59] H. Yokoyama, M. Okamoto, Y. Osaka, Jpn. J. Appl. Phys. 30 (1991) 344.
[60] M. Friedrich, J. Hahn, S. Laufer, F. Richter, H.-J. Hinneberg, D.R.T. Zahn, in: K.V. Ravi, K.E. Spear, J.L. Davidson, R.H. Hauge, J.P. Dismukes (eds.), Diamond Materials IV Electrochemical Society Proc., Vol. 94/95, The Electrochemical Society, Pennington, NJ, 1995.
[61] D.R. McKenzie, W.D. McFall, W.G. Sainty, C.A. Davis, R.E. Collins, Diamond Relat. Mater. 2 (1993) 970–976.
[62] S. Fahy, Phys. Rev. B 51 (1995) 12873.
[63] S. Fahy, Phys. Rev. B 53 (1996) 11884.
[64] See also M. Cardona, E. Anastassakis, Phys. Rev. B 54 (1996) 14888.
[65] L.B. Hackenberger, L.J. Pilione, R. Messier, G.P. Lamaze, J. Vac. Sci. Technol. A 12 (1994) 1569.
[66] S. Fahy, C.A. Taylor II, R. Clarke, Phys. Rev. B (1997), submitted.
[67] W. Gissler, J. Haupt, T.A. Crabb, P.N. Gibson, D.G. Rickerby, Mater. Sci. Engin. A 139 (1991) 284.
[68] W. Dworschak, K. Jung, H. Ehrhardt, Diamond Relat. Mater. 3 (1994) 337.
[69] Joint Committee on Powder Diffraction Standards, JCPDS, Swarthmore, PA, pattern 25-1033.
[70] Y.G. Andreev, T. Lundstrom, J. Appl. Cryst. 27 (1994) 767.
[71] C.R. Aita, in: J.J. Pouch, S.A. Alterovitz (eds.), Synthesis and Properties of Boron Nitride, Materials Science Forum, Vol. 54/55, Trans Tech Publications, Brookfield, 1990, p. 1.
[72] V.Y. Kulikovsky, L.R. Shaginyan, V.M. Vereschaka, N.G. Hatyenko, Diamond Relat. Mater. 4 (1995) 113.
[73] G.L. Doll, T.A. Perry, J.A. Sell, in: H.A. Atwater, F.A. Houle, D.H. Lowndes (eds.), Surface Chemistry and Beam-Solid Interactions, Vol. 201, Materials Research Society, Pittsburgh, PA, 1991, p. 207.
[74] Joint Committee on Powder Diffraction Standards, JCPDS, Swarthmore, PA, pattern 34-421.
[75] Joint Committee on Powder Diffraction Standards, JCPDS, Swarthmore, PA, pattern 12-377.
[76] B.D. Cullity, Elements of X-Ray Diffraction, 2nd edn., Addison–Wesley, Reading, MA, 1978.
[77] D.G. Rickerby, P.N. Gibson, W. Gissler, J. Haupt, Thin Solid Films 209 (1992) 155.
[78] S. Kidner, C.A. Taylor II, R. Clarke, Appl. Phys. Lett. 64 (1994) 1859.
[79] A.K. Ballal, L. Salamanca-Riba, C.A. Taylor II, G.L. Doll, Thin Solid Films 224 (1993) 46.
[80] D.L. Medlin, T.A. Friedmann, P.B. Mirkarimi, P. Rez, K.F. McCarty, M.J. Mills, J. Appl. Phys. 76 (1994) 295.
[81] L.F. Allard, A.K. Datye, T.A. Nolan, S.L. Mahan, R.T. Paine, Ultramicroscopy 37 (1991) 153.
[82] S. Turan, K.M. Knowles, Phys. Status Solidi 150 (1995) 227.
[83] D.L. Medlin, T.A. Friedmann, P.B. Mirkarimi, M.J. Mills, F.M. K, Phys. Rev. B 50 (1994) 7884.
[84] D.J. Smith, W.O. Saxton, M.A. O'Keefe, G.J. Wood, W.M. Stobbs, Ultramicroscopy 11 (1983) 263.
[85] K.F. McCarty, M.J. Mills, D.L. Medlin, T.A. Friedmann, Phys. Rev. B 50 (1994) 8907.
[86] H.K. Schmid, Microsc. Microanal. Microstruct. 6 (1995) 99.
[87] C.A. Davis, K.M. Knowles, G.A.J. Araratunga, Surf. Coat. Technol. 76 (1995) 316.

[88] D.A. Muller, Y. Tzou, R. Raj, J. Silcox, Nature 366 (1993) 725.
[89] G. Sené, D. Bouchier, S. Ilias, M.A. Djouadi, V. Stambouli, P. Möller, G. Hug, S. Reinke, unpublished work, 1996.
[90] O. Burat, D. Bouchier, V. Stambouli, G. Gautherin, J. Appl. Phys. 68 (1990) 2780.
[91] W.B. Sainty, P.J. Martin, R.P. Netterfield, D.R. McKenzie, D.J.H. Cockayne, D.M. Dwarte, J. Appl. Phys. 64 (1988) 3980.
[92] R. Trehan, Y. Lifshitz, J.W. Rabalais, J. Vac. Sci. Technol. A 8 (1990) 4026.
[93] A. Weber, U. Bringmann, R. Nikulski, C.P. Klages, Diamond Relat. Mater. 2 (1993) 201.
[94] G.P. Lamaze, R.G. Downing, L.B. Hackenberger, L.J. Pilione, R. Messier, Diamond Relat. Mater. 3 (1994) 728.
[95] T. Werninghaus, J. Hahn, F. Richter, D.R.T. Zahn, Appl. Phys. Lett. 70 (1997) 958.
[96] J.W. Robinson, Handbook of Spectroscopy, Vol. 2, CRC Press, Cleveland, OH, 1974, p. 108.
[97] A. Chaiken, L.J. Terminello, J. Wong, G.L. Doll, C.A. Taylor II, Appl. Phys. lett. 63 (1993) 2112.
[98] L.J. Terminello, A. Chaiken, D.A. Lapiano-Smith, G.L. Doll, T. Sato, J. Vac. Sci. Technol. 12 (1994) 2462.
[99] M. Jaouen, G. Hug, V. Gonnet, G. Demazeau, G. Tourillon, Microsc. Microanal. Microstruc. 6 (1995) 127.
[100] O. Stenzel, J. Hahn, M. Röder, A. Ehrlich, S. Prause, F. Richter, Phys. Status Solidi A 158 (1996) 281.
[101] H. Hofsäss, H. Feldermann, M. Sebastian, C. Ronning, Phys. Rev. B55 (1997) 13230.
[102] T. Ishii, T. Sato, J. Crystal Growth 61 (1983) 689.
[103] K. Inagawa, K. Watanabe, H. Ohsone, K. Saitoh, A. Itoh, J. Vac. Sci. Technol. A 5 (1987) 2696.
[104] T. Ikeda, Y. Kawate, Y. Hirai, J. Vac. Sci. Technol. A 8 (1990) 3168.
[105] D.J. Kester, R. Messier, J. Appl. Phys. 72 (1992) 504.
[106] T. Ikeda, Appl. Phys. Lett. 61 (1992) 786.
[107] N. Tanabe, T. Hayashi, M. Iwaki, Diamond Relat. Mater. 1 (1992) 151.
[108] P.B. Mirkarimi, K.F. McCarty, D.L. Medlin, W.G. Wolfer, T.A. Friedmann, E.J. Klaus, G.F. Cardinale, D.G. Howitt, J. Mater. Res. 9 (1994) 2925.
[109] D. Bouchier, G. Sené, M.A. Djouadi, P. Möller, Nucl. Instrum. Meth. B 89 (1994) 369.
[110] R. Ganzetti, W. Gissler, Mater. Manuf. Processes 9 (1994) 507.
[111] S. Reinke, M. Kuhr, W. Kulisch, Diamond Relat. Mater. 3 (1994) 341.
[112] S. Reinke, M. Kuhr, W. Kulisch, Surf. Coat. Technol. 74/75 (1995) 723.
[113] S. Reinke, M. Kuhr, W. Kulisch, R. Kassing, Diamond Relat. Mater. 4 (1995) 272.
[114] J.D. Targove, H.A. Macleod, Appl. Opt. 27 (1988) 3779.
[115] H. Kawashima, N. Shibata, Jpn. J. Appl. Phys. 34 (1995) 5758.
[116] S. Ulrich, J. Schwan, W. Donner, H. Ehrhardt, Diamond Relat. Mater. 5 (1996) 548.
[117] M.P. Johansson, I. Ivanoz, L. Hultman, P. Munger, A. Schütze, J. Vac. Sci. Tecnol. A 14 (1996) 3100.
[118] D.J. Kester, R. Messier, Mater. Res. Soc. Symp. Proc. 235 (1992) 721.
[119] M. Kuhr, S. Reinke, W. Kulisch, Surf. Coat. Technol. 74/75 (1995) 806.
[120] G. Sené, D. Bouchier, S. Ilias, M.A. Djouadi, J. Pascallon, V. Stambouli, P. Möller, G. Hug, Diamond Relat. Mater. 5 (1996) 530.
[121] C.A. Taylor II, R. Clarke, Appl. Phys. Lett. (1997), submitted.
[122] D.R. McKenzie, W.D. McFall, H. Smith, B. Higgins, R.W. Boswell, A. Durandet, B.W. James, I.S. Falconer, Nucl. Instrum. Meth. B 106 (1995) 90.
[123] J. Hahn, F. Richter, R. Pintaske, M. Röder, E. Schneider, T. Welzel, Surf. Coat. Technol. 92 (1996) 129.
[124] M. Sueda, T. Kobayashi, H. Tsukamoto, T. Rokkaku, S. Morimoto, Y. Fukaya, N. Yamashita, T. Wada, Thin Solid Films 228 (1993) 97.
[125] J.P. Biersack, L.G. Haggmark, Transport of Ions in Matter program, Nuclear Instruments and Methods 174 (1980) 257–269.
[126] J.F. Ziegler, J.P. Biersak, U. Littmark, The Stopping and Range of Ions in Solids, Pergamon Press, New York, 1985.
[127] P.B. Mirkarimi, D.L. Medlin, K.F. McCarty, J.C. Barbour, Appl. Phys. Lett. 66 (1995) 2813.
[128] K. Bewilogua, J. Buth, H. Hubsch, M. Grischke, Diamond Relat. Mater. 2 (1993) 1206.
[129] M. Mieno, T. Yoshida, Jpn. J. Appl. Phys. 29 (1990) L1175.
[130] T. Wada, N. Yamashita, J. Vac. Sci. Technol. A10 (1992) 515.
[131] Y. Andoh, K. Ogata, E. Kamijo, Nucl. Instrum. Meth. 33 (1988) 678.
[132] H. Hofsäss, C. Ronning, U. Griesmeier, M. Gross, S. Reinke, M. Kuhr, Appl. Phys. Lett. 67 (1995) 46.
[133] D.J. Kester, K.S. Ailey, D.J. Lichtenwalner, R.F. Davis, J. Vac. Sci. Technol. A 12 (1994) 3074.
[134] P.X. Yan, S.Z. Yang, B. Li, X.S. Chen, J. Cryst. Growth 148 (1995) 232.
[135] W.L. Lin, Z. Xia, Y.L. Liu, Y.C. Fen, Mater. Sci. Engin. B 7 (1990) 107.
[136] J.J. Cuomo, J.P. Doyle, J. Bruley, J.C. Liu, Appl. Phys. Lett. 58 (1991) 466.
[137] P.B. Mirkarimi, D.L. Medlin, K.F. McCarty, D.C. Dibble, W.M. Clift, J.A. Knapp, J.C. Barbour, J. Appl. Phys. 82 (1997) 1617.
[138] M.J. Paisley, L.P. Bourget, R.F. Davis, Thin Solid Films 235 (1993) 30.
[139] H. Lüthje, K. Bewilogua, S. Daaud, M. Johansson, L. Hultman, Thin Solid Films 257 (1995) 40.
[140] M. Okamato, H. Yokoyama, Y. Osaka, Jpn. J. Appl. Phys. 29 (1990) 930.
[141] M. Okamoto, Y. Utsumi, Y. Osaka, Jpn. J. Appl. Phys. 29 (1990) L1004.

[142] F. Zhang, Y. Guo, Z. Song, G. Chen, Appl. Phys. Lett. 65 (1994) 971.
[143] M. Murakawa, S. Watanabe, Surf. Coat. Technol. 43/44 (1990) 145.
[144] S. Shanfield, R. Wolfson, J. Vac. Sci. Technol. A 1 (1983) 323.
[145] S. Nishiyama, N. Kuratani, A. Ebe, K. Ogata, Nucl. Instrum. Meth. B 80/81 (1993) 1485.
[146] T. Ikeda, T. Satou, H. Satoh, Surf. Coat. Technol. 50 (1991) 33.
[147] M. Murakawa, S. Watanabe, Surf. Coat. Technol. 43/44 (1990) 128.
[148] T. Ikeda, Appl. Phys. Lett. 61 (1992) 786.
[149] S. Watanabe, S. Miyake, M. Murakawa, Surf. Coat. Technol. 49 (1991) 406.
[150] M. Lu, A. Bousetta, R. Sukach, A. Bensaoula, K. Walters, K. Eipers-Smith, A. Schultz, Appl. Phys. Lett. 64 (1994) 1514.
[151] S. Mineta, M. Kolrata, N. Yasunaga, Y. Kikuta, Thin Solid Films 189 (1990) 125.
[152] A.K. Ballal, L. Salamanca-Riba, G.L. Doll, C.A. Taylor II, R. Clarke, J. Mater. Res. 7 (1992) 1618.
[153] E.V. Pechen, A.V. Varlashkin, S.I. Krasnosvobodtsev, B. Brunner, K.F. Renk, Appl. Phys. Lett. 66 (1995) 2292.
[154] M.D. Wiggins, C.R. Aita, F.S. Hickernell, J. Vac. Sci. Technol. A 2 (1984) 322.
[155] W. Gissler, J. Haupt, A. Hoffmann, P.N. Gibson, D.G. Rickerby, Thin Solid Films 199 (1991) 113.
[156] M. Mieno, T. Yoshida, Surf. Coat. Technol. 52 (1992) 87.
[157] J. Hahn, M. Friedrich, R. Pintaske, M. Schaller, N. Kahl, D.R.T. Zahn, F. Richter, Diamond Relat. Mater. 5 (1996) 1103.
[158] A. Schütze, K. Bewilogua, H. Lüthje, S. Kouptsidas, S. Jäger, Surf. Coat. Technol. 74/75 (1995) 717.
[159] N. Tanabe, M. Iwaki, Nucl. Instrum. Meth. B 80/81 (1993) 1349.
[160] M.P. Johansson, L. Hultman, S. Daaud, K. Bewilogua, H. Lüthje, A. Schütze, S. Kouptsidas, G.S.A.M. Theunissen, Thin Solid Films 287 (1996) 193.
[161] P.B. Mirkarimi, unpublished work, 1996.
[162] A. Chayahara, H. Yokoyama, T. Imura, Y. Osaka, Jpn. J. Appl. Phys. 26 (1987) L1435.
[163] A. Chayahara, H. Yokoyama, T. Imura, Y. Osaka, Appl. Surf. Sci. 33/34 (1988) 561.
[164] H. Saitoh, T. Hirose, H. Matsui, Y. Hirotsu, Y. Ichinose, Surf. Coat. Technol. 39/40 (1989) 265.
[165] Y. Osaka, A. Chayahara, H. Yokoyama, M. Okamoto, T. Hamada, T. Imura, M. Fujisawa, in: J.J. Pouch, S.A. Alterovitz (eds.), Synthesis and Properties of Boron Nitride, Materials Science Forum, Vol. 54/55, Trans Tech Publications, Brookfield, 1990.
[166] T. Ichiki, T. Momose, T. Yoshida, J. Appl. Phys. 75 (1994) 1330.
[167] M. Okamoto, Y. Utsumi, Y. Osaka, Plasma Sources Sci. Technol. 2 (1993) 1.
[168] K.J. Liao, W.L. Wang, Phys. Stat. Sol. 147 (1995) K9.
[169] H. Saitoh, W.A. Yarbrough, Appl. Phys. Lett. 58 (1991) 2230.
[170] S. Komatsu, Y. Moriyoshi, M. Kasamatsu, K. Yamada, J. Phys. D 24 (1991) 1687.
[171] M.Z. Karim, D.C. Cameron, M.J. Murphy, M.J. Hashimi, Surf. Coat. Technol. 49 (1991) 416.
[172] M.Z. Karim, D.C. Cameron, M.S.J. Hashimi, Surf. Coat. Technol. 54/55 (1992) 355.
[173] D.C. Cameron, M.Z. Karim, M.S.J. Hashimi, Thin Solid Films 236 (1993) 96.
[174] T. Ichiki, S. Amagi, T. Yoshida, J. Appl. Phys. 79 (1996) 4381.
[175] M.F. Plass, W. Fukarek, A. Kolitsch, M. Mäder, W. Möller, Phys. Stat. Sol. A 155 (1996) K1.
[176] D.H. Berns, M.A. Cappelli, Appl. Phys. Lett. 68 (1996) 2711.
[177] G. Krannich, F. Richter, J. Hahn, R. Pintaske, V.B. Filippov, Y. Paderno, Diamond Relat. Mater. 6 (1997) 1005.
[178] F. Richter, G. Krannich, J. Hahn, R. Pintaske, M. Friedrich, S. Schmidbauer, D.R.T. Zahn, Surf. Coat. Technol. 90 (1996) 178.
[179] S. Manorama, G.N. Chaudhari, V.J. Rao, J. Phys. D 26 (1993) 1793.
[180] A.R. Phani, G.N. Chaudhari, S. Manorama, J. Solid State Chem. 118 (1995) 99.
[181] A.R. Phani, S. Roy, V.J. Rao, Thin Solid Films 258 (1995) 21.
[182] G.L. Doll, J.A. Sell, C.A. Taylor II, R. Clarke, Phys. Rev. B 43 (1991) 6816.
[183] R. Clarke, C.A. Taylor II, G.L. Doll, T.A. Perry, Diamond Relat. Mater. 1 (1992) 93.
[184] T.A. Friedmann, K.F. McCarty, E.J. Klaus, D. Boehme, W.M. Clift, H.A. Johnsen, M.J. Mills, D.K. Ottesen, Appl. Phys. Lett. 61 (1992) 2406.
[185] R.W. Pryor, Z.L. Wu, K.R. Padmanabhan, S. Villanueva, R.L. Thomas, Thin Solid Films 253 (1994) 243.
[186] R.W. Pryor, K.R. Padmanabhan, K. Chawla, Diamond Relat. Mater. 4 (1995) 128.
[187] F. Qian, V. Nagabushnam, R.K. Singh, Appl. Phys. Lett. 63 (1993) 317.
[188] P.A. Molian, J. Mater. Sci. 29 (1994) 5646.
[189] W.A. Yarbrough, R. Messier, Science 247 (1990) 688.
[190] T. Klotzbucher, W. Pflenging, M. Mertin, D.A. Wesner, E.W. Kreutz, Appl. Surf. Sci. 86 (1995) 165.
[191] W. Pfleging, T. Klotzbucher, D.A. Wesner, E.W. Kreutz, Diamond Relat. Mater. 4 (1995) 370.
[192] J. Narayan, H. Wu, R.D. Vispute, J. Electronic Mater. 25 (1996) 143.
[193] K. Inagawa, K. Watanabe, K. Saitoh, Y. Yuchi, A. Itoh, Surf. Coat. Technol. 39/40 (1989) 253.
[194] W.D. Halverson, T.G. Tetreault, J.K. Hirvonen, in: J.J. Pouch, S.A. Alterovitz (eds.), Synthesis and Properties of Boron Nitride, Materials Science Forum, Vol. 54/55, Trans Tech Publications, Brookfield, 1990, p. 71.

[195] D.J. Kester, K.S. Ailey, R.F. Davis, Diamond Relat. Mater. 3 (1994) 332.
[196] H. Hofsäss, C. Ronning, U. Griesmeier, M. Gross, S. Reinke, M. Kuhr, J. Zweck, R. Fischer, Nucl. Instrum. Meth. B 106 (1995) 153.
[197] G.F. Cardinale, P.B. Mirkarimi, K.F. McCarty, E.J. Klaus, D.L. Medlin, W.M. Clift, D.G. Howitt, Thin Solid Films 253 (1994) 130.
[198] D.G. McCulloch, D.R. McKenzie, S. Prawer, Philos. Mag. A 72 (1995) 1031.
[199] D.R. McKenzie, J. Vac. Sci. Technol. B 11 (1993) 1928.
[200] G.F. Cardinale, D.L. Medlin, P.B. Mirkarimi, K.F. McCarty, D.G. Howitt, J. Vac. Sci. Technol. A 15 (1997) 196.
[201] K.F. McCarty, D.L. Medlin, Diamond Relat. Mater. 6 (1997) 1219.
[202] D.S. Zhou, C.L. Chen, T.E. Mitchell, L.B. Hackenberger, R. Messier, Philos. Mag. Lett. 72 (1995) 163.
[203] H. Yamashita, K. Kuroda, H. Saka, N. Yamashita, T. Watanabe, T. Wada, Thin Solid Films 253 (1994) 72.
[204] W.L. Zhou, Y. Ikuhara, M. Murakawa, S. Watanabe, T. Suziki, Appl. Phys. Lett. 66 (1995) 2490.
[205] W.L. Zhou, Y. Ikuhara, T. Suzuki, Appl. Phys. Lett. 67 (1995) 3551.
[206] D.L. Medlin, T.A. Friedmann, P.B. Mirkarimi, G.F. Cardinale, K.F. McCarty, J. Appl. Phys. 79 (1996) 3567.
[207] D.R. McKenzie, W.D. McFall, S. Reisch, B.W. James, I.S. Falconer, R.W. Boswell, H. Persing, A.J. Perry, A. Durandet, Surf. Coat. Technol. 78 (1996) 255.
[208] K. Bewilogua, A. Schütze, S. Kouptsidis, H. Lüthje, in: A. Feldman, Y. Tzeng, W.A. Yarbrough, M. Yoshikawa, M. Murakawa (eds.), Applications of Diamond films and Related Materials: Third International Conference, NIST Special Publication 885, 1995, p. 831.
[209] S. Reinke, M. Kuhr, W. Kulisch, in: K.V. Ravi, K.E. Spear, J.L. Davidson, R.H. Hauge, J.P. Dismukes (eds.), Diamond Materials IV Electrochemical Society Proc., Vol. 94/95, The Electrochemical Society, Diamond Materials IV Electrochemical Society Proc., 1995.
[210] R.M. Wentzcovitch, S. Fahy, M.L. Cohen, S.G. Louie, Phys. Rev. B 38 (1988) 6191.
[211] J.K. Dubray, C.G. Pantano, W.A. Yarbrough, J. Appl. Phys. 72 (1992) 3136.
[212] Z. Li, L. Wang, T. Suzuki, A. Argoitia, P. Pirouz, J.C. Angus, J. Appl. Phys. 73 (1993) 711.
[213] T. Suzuki, M. Yagi, K. Shibuki, M. Hasemi, Appl. Phys. Lett. 65 (1994) 540.
[214] W.R.L. Lambrecht, C.H. Lee, B. Segall, J.C. Angus, Z. Li, M. Sunkara, Nature 364 (1993) 607.
[215] J. Widany, T. Frauenheim, W.R.L. Lambrecht, J. Mater. Chem. 6 (1996) 899.
[216] K.S. Park, D.Y. Lee, K.J. Kim, D.W. Moon, Appl. Phys. Lett. 70 (1997) 315.
[217] A.V. Hamza, G.D. Kubiak, R.H. Stulen, Surface Science 237 (1990) 35.
[218] Chem. Eng. News, Dec. 17, 1990, p. 28.
[219] A. Argoita, J.C. Angus, J.S. Ma, L. Wang, P. Pirouz, W.R.L. Lambrecht, J. Mater. Res. 9 (1994) 1849.
[220] K.F. McCarty, M.J. Mills, D.L. Medlin, T.A. Friedmann, Phys. Rev. B 50 (1994) 8907.
[221] J. Robertson, Diamond Relat. Mater. 5 (1996) 519.
[222] J. Malherbe, Crit. Rev. Sol. State 19 (1994) 55.
[223] F. Seitz, J.S. Koehler, in Progress in Solid State Physics, Vol. 2, Academic Press, New York, 1954, p. 30.
[224] C. Weissmantel, K. Bewilogua, D. Dietrich, H.-J. Erler, H.-J. Hinneberg, S. Klose, W. Nowick, G. Reisse, Thin Solid Films 72 (1980) 19.
[225] C. Weissmantel, J. Vac. Sci. Technol. 18 (1981) 179.
[226] C. Weissmantel, Thin Solid Films 92 (1982) 55.
[227] T. Díaz de la Rubia, Ann. Rev. Mater. Science 26 (1996) 613.
[228] T. Díaz de la Rubia, personal communication.
[229] G.F. Cardinale, D.G. Howitt, K.F. McCarty, D.L. Medlin, P.B. Mirkarimi, N.R. Moody, Diamond Relat. Mater. 5 (1996) 1295.
[230] S. Reinke, M. Kuhr, W. Kulisch, Diamond Relat. Mater. 5 (1996) 508.
[231] R. Berman, F. Simon, Z. Elektrochem. 59 (1955) 333.
[232] M.K. Puchert, P.Y. Timbrell, R.N. Lamb, D.R. McKenzie, J. Vac. Sci. Technol. A 12 (1994) 727.
[233] F.M. D'Heurle, Metall. Trans. 1 (1970) 725.
[234] H. Windischmann, J. Vac. Sci. Technol. A 9 (1991) 2431.
[235] H. Windischmann, Crit. Rev. Solid State 17 (1992) 547.
[236] H. Windischmann, J. Appl. Phys. 62 (1987) 1800.
[237] P. Sigmund, in Sputtering by Particle Bombardment, Vol. 1, ed. R. Behrisch, Springer, Berlin, 1981, p. 49.
[238] C.A. Davis, Thin Solid Films 226 (1993) 30.
[239] J. Robertson, Diamond Relat. Mater. 2 (1993) 984.
[240] Y. Lifshitz, S.R. Kasi, J.W. Rabalais, Phys. Rev. Lett. 62 (1987) 1290.
[241] Y. Lifshitz, S.R. Kasi, J.W. Rabalais, Phys. Rev. B 41 (1990) 10468.
[242] J. Robertson, Diamond Relat. Mater. 3 (1994) 361.
[243] M. Nastasi, J.W. Mayer, Materials Science Reports 6 (1991) 1.
[244] D.L. Pappas, K.L. Saenger, J. Bruley, W. Krakow, J.J. Cuomo, T. Gu, R.W. Collins, J. Appl. Phys. 71 (1992) 5675.
[245] D.R. McKenzie, D. Muller, B.A. Pailthorpe, Phys. Rev. Lett. 67 (1991) 773.
[246] B.W. Mott, Micro-Indentation Hardness Testing, Buttersworth Scientific, London, 1956.

[247] P.J. Blau, B.R. Lawn, Microindentation Techniques in Materials Science and Engineering, ASTM Special Technical Publication 889, ASTM, Philadelphia, PA, 1985.
[248] T. Taniguchi, M. Akaishi, S. Yamaoka, J. Amer. Ceram. Soc. 79 (1996) 547.
[249] N.V. Novikov, Y.A. Sirota, V.I. Mal'nev, I.A. Petrusha, Diamond Relat. Mater. 2 (1993) 1253.
[250] C.A. Brookes, in: J.E. Field (ed.), The Properties of Natural and Synthetic Diamond, Academic Press, London, 1992, p. 515.
[251] V.B. Shipilo, E.M. Shishonok, E.M. Zaitsev, N.G. Anichenko, L.S. Unyarkha, Inorg. Mater. 26 (1990) 1401.
[252] V.K. Nurmukhamedov, G.A. Adler, V.I. Veprintsev, N.A. Luchsheva, V.A. Botsulyak, Inorg. Mater. 14 (1978) 1497.
[253] E. Knittle, R.M. Wentzcovitch, R. Jeanloz, M.L. Cohen, Nature 337 (1989) 6205.
[254] V.I. Aleksandrov, A.P. Goncharov, I.N. Makarenko, A.N. Zisman, E.V. Jakovenko, S.M. Stishov, High Pressure Res. 1 (1989) 333.
[255] M. Grimsditch, E.S. Zouboulis, A. Polian, J. Appl. Phys. 76 (1994) 832.
[256] C.A. Brookes, in: E.A. Almond, C.A. Brookes, R. Warren (eds.), Proc. Int. Conf. on Science of Hard Materials, Inst. Phys. Conf. Series No. 75, Adam Hilger, Bristol, 1986.
[257] P. Rodriguez-Hernandez, M. Gonzalez-Diaz, A. Munoz, Phys. Rev. B 51 (1995) 14 705.
[258] K. Kim, W.R.L. Lambrecht, B. Segall, Phys. Rev. B 53 (1996) 16310.
[259] P.K. Mehrota, D.T. Quinto, G.J. Wolfe, Proc. 9th Int. Conf. on CVD, The Electrochemical Society, Pennington, NJ, 1984, p. 757.
[260] C. Feldman, F. Ordway, J. Bernstein, J. Vac. Sci. Technol. A 8 (1990) 117.
[261] S.V. Hainsworth, T.F. Page, in: W.W. Gerberich, H. Gao, J.-E. Sundgren, S.P. Baker (eds.), Materials Research Society Proceedings, Vol. 436, Materials Research Society, Pittsburgh, PA, 1997.
[262] S.J. Bull, P.R. Chalker, C. Johnston, Mater. Sci. Technol. 8 (1992) 679.
[263] Y. Andoh, S. Nishiyama, H. Kirimura, T. Mikami, K. Ogata, F. Fujimoto, Nucl. Instrum. Meth. B 59/60 (1991) 276.
[264] D.R. McKenzie, personal communicaton.
[265] M.P. Johansson, H. Sjöström, L. Hultman, J. Mater. Res. (1996), submitted.
[266] W.C. Oliver, G.M. Pharr, J. Mater. Res. 7 (1992) 1564.
[267] M. Lu, A. Bousetta, A. Bensaoula, K. Walters, J.A. Schultz, Appl. Phys. Lett. 68 (1996) 622.
[268] R.F. Davis, III-V Nitrides for Electronic and Optoelectronic Applications, Proceedings of IEEE 79 (1991) 702.
[269] O. Mishima, J. Tanaka, S. Yamaoka, O. Fukunaga, Science 238 (1987) 181.
[270] C. Ronning, E. Dreher, H. Feldermann, M. Sebastian, H. Hofsäss, Diamond Relat. Mater. 6 (1997) 1129.
[271] H. Morkoç, S. Strite, G.B. Gao, M.E. Lin, B. Sverdlov, M. Burns, J. Appl. Phys. 76 (1994) 1363.
[272] M.P. Surh, S.G. Louie, M.L. Cohen, Phys. Rev. B 43 (1991) 9126.
[273] J. Szmidt, A. Werbowy, A. Michalski, A. Olszyna, A. Sokolowska, S. Mitura, Diamond Relat. Mater. 4 (1995) 1131.
[274] J. Szmidt, Diamond Relat. Mater. 3 (1994) 650.
[275] J. Szmidt, Diamond Relat. Mater. 1 (1992) 681.
[276] T. Brozek, J. Szmidt, A. Jakubowski, A. Olszyna, Diamond Relat. Mater. 3 (1994) 720.
[277] J. Szmidt, A. Jakubowski, A. Michalski, A. Rusek, Thin Solid Films 110 (1983) 7.
[278] M. Sokolowski, A. Sokolowska, A. Michalski, Z. Romanowski, A. Rusek-Mazurek, M. Wronikowski, Thin Solid Films 80 (1981) 249.
[279] A.R. Phani, S. Manorama, V.J. Rao, Semicond. Sci. Technol. 10 (1995) 1520.
[280] V.A. Gubanov, L.A. Hemstreet, C.Y. Fong, B.M. Klein, Appl. Phys. Lett. 69 (1996) 227.
[281] V.A. Gubanov, Z.W. Lu, B.M. Klein, C.Y. Fong, Phys. Rev. B 53 (1996) 4377.
[282] M.Z. Karim, D.C. Cameron, in Proceedings of 5th SiC and Relat. Mater. Conf., Inst. Phys. Conf. Ser. No. 137, Washington, DC, 1993.
[283] O. Madelung, W. von der Oster, U. Rössler, in Landolt–Börnstein: Numerical Data and Functional Relationaships in Science and Technology, Vol. 22a, Springer–Verlag, Berlin, 1989.
[284] J.P. Sullivan, T.A. Friedmann, C.A. Apblett, M.P. Siegal, N. Missert, M.L. Lovejoy, P.B. Mirkarimi, K.F. McCarty, in Materials Research Society Proceedings, Vol. 381, Materials Research Society, Pittsburgh, 1995.
[285] M.J. Rand, J.F. Roberts, J. Electrochem Soc. 115 (1968) 423.
[286] M.F. Doerner, W.D. Nix, Crit. Rev. Sol. State 14 (1988) 225.
[287] H. Kohzuki, Y. Okuno, M. Motoyama, Diamond Films Technol. 5 (1995) 95.
[288] W.D. McFall, D.R. McKenzie, R.P. Netterfield, Surf. Coat. Technol. 81 (1996) 72.
[289] J.V. Busch, J.P. Dismukes, Diamond Relat. Mater. 3 (1994) 295.
[290] K.F. McCarty, unpublished work.